Cyclipostins and cyclophostin analogs inhibit the antigen 85C from Mycobacterium tuberculosis both in vitro and in vivo

Albertus Viljoen, Matthias Richard, Phuong Chi Nguyen, Patrick Fourquet, Luc Camoin, Rishi R. Paudal, Giri R Gnawali, Christopher D Spilling, Jean-François Cavalier, Stéphane Canaan, et al.

Cyclipostins and cyclophostin analogs inhibit the antigen 85C from *Mycobacterium tuberculosis* both *in vitro* and *in vivo*

Received for publication, November 2, 2017, and in revised form, December 5, 2017 Published, Papers in Press, January 4, 2018, DOI 10.1074/jbc.RA117.000760

Albertus Viljoen[‡1], Matthias Richard[‡1], Phuong Chi Nguyen[§¶2], Patrick Fourquet[‖], Luc Camoin[‖], Rishi R. Paudal[**], Giri R. Gnawali[**], Christopher D. Spilling[**], Jean-François Cavalier[§¶], Stéphane Canaan[§¶], Mickael Blaise[‡3], and Laurent Kremer[‡ ‡‡4]

From the [‡]Institut de Recherche en Infectiologie de Montpellier (IRIM), Université de Montpellier, CNRS UMR9004, 34293 Montpellier, France, [‡‡]INSERM, IRIM, 34293 Montpellier, France, [§]Aix-Marseille Université, CNRS, EIPL, IMM FR3479, 13009 Marseille, France, [¶]Aix-Marseille Université, CNRS, LISM, IMM FR3479, 13009 Marseille, France, [‖]Aix Marseille Université, CNRS, INSERM, Institut Paoli-Calmettes, CRCM, Marseille Protéomique, 13009 Marseille, France, and the [**]Department of Chemistry and Biochemistry, University of Missouri, St. Louis, Missouri 63121

Edited by Chris Whitfield

An increasing prevalence of cases of drug-resistant tuberculosis requires the development of more efficacious chemotherapies. We previously reported the discovery of a new class of cyclipostins and cyclophostin (CyC) analogs exhibiting potent activity against *Mycobacterium tuberculosis* both *in vitro* and in infected macrophages. Competitive labeling/enrichment assays combined with MS have identified several serine or cysteine enzymes in lipid and cell wall metabolism as putative targets of these CyC compounds. These targets included members of the antigen 85 (Ag85) complex (*i.e.* Ag85A, Ag85B, and Ag85C), responsible for biosynthesis of trehalose dimycolate and mycolylation of arabinogalactan. Herein, we used biochemical and structural approaches to validate the Ag85 complex as a pharmacological target of the CyC analogs. We found that $CyC_{7\beta}$, $CyC_{8\beta}$, and CyC_{17} bind covalently to the catalytic Ser^{124} residue in Ag85C; inhibit mycolyltransferase activity (*i.e.* the transfer of a fatty acid molecule onto trehalose); and reduce triacylglycerol synthase activity, a property previously attributed to Ag85A. Supporting these results, an X-ray structure of Ag85C in complex with $CyC_{8\beta}$ disclosed that this inhibitor occupies Ag85C's substrate-binding pocket. Importantly, metabolic labeling of *M. tuberculosis* cultures revealed that the CyC compounds impair both trehalose dimycolate synthesis and mycolylation of arabinogalactan. Overall, our study provides compelling evidence that CyC analogs can inhibit the activity of the Ag85 complex *in vitro* and in mycobacteria, opening the door to a new strategy for inhibiting Ag85. The high-resolution crystal structure obtained will further guide the rational optimization of new CyC scaffolds with greater specificity and potency against *M. tuberculosis*.

This work was supported by Fondation pour la Recherche Médicale (FRM) Grants DEQ20150331719 (to L. K.) and ECO20160736031 (to M. R.) and by CNRS and INSERM. The authors declare that they have no conflicts of interest with the contents of this article.

The atomic coordinates and structure factors (code 5OCJ) have been deposited in the Protein Data Bank (http://wwpdb.org/).

[1] Both authors contributed equally to this work.

[2] Supported by the Ph.D. Training program of the University of Science and Technology of Hanoi.

[3] To whom correspondence may be addressed. Tel.: 33-4-34-35-94-47; E-mail: mickael.blaise@irim.cnrs.fr.

[4] To whom correspondence may be addressed. Tel.: 33-4-34-35-94-47; E-mail: laurent.kremer@irim.cnrs.fr.

With 10.4 million new cases and 1.8 million deaths in 2016, tuberculosis (TB)[5] continues to be a major global health problem. TB is caused by *Mycobacterium tuberculosis*, a resilient microorganism that persists through long courses of antibiotics and years of dormancy within the host. The emergence of multidrug-resistant and extensively drug-resistant TB has contributed to the difficulties in treating this bacterial infection (1). Chemotherapeutic treatments against TB remain very challenging and complicated, essentially because of the slow rate of growth of the bacilli and the presence of a thick, greasy, and relatively drug-impermeable cell wall (2). This mycobacterial cell wall consists of a complex skeleton comprising covalently linked macromolecules, such as peptidoglycan, arabinogalactan, and mycolic acids, in which non-covalently associated glycolipids are interspersed (3). The mycolic acid portion of the envelope is composed of very long fatty acids (C70–90) that are either covalently attached to the arabinan moiety of the arabinogalactan (AG) polymer or found esterified to trehalose as trehalose monomycolate (TMM) or trehalose dimycolate (TDM). Because several key antitubercular drugs, such as isoniazid, SQ109, delamanid, or ethambutol, target different aspects of the biosynthetic steps responsible for the cell wall attachment of mycolic acids (4–7), this pathway is of particular interest from a drug discovery perspective.

The three functionally and structurally related members of the antigen 85 complex, designated Ag85A, -B, and -C, are among the most abundantly secreted proteins in *M. tuberculosis* (8). These enzymes are responsible for the biosynthesis of TMM and TDM as well as the covalent attachment of mycolic acids to AG (9–11). Deletion of *fbpC2*, encoding Ag85C, resulted in a 40% decrease in the AG-bound mycolic acids but failed to affect the production of non-covalently linked myco-

[5] The abbreviations used are: TB, tuberculosis; AG, arabinogalactan; CyC, cyclipostins and cyclophostin; DGAT, diacylglycerol acyltransferase; FAME, fatty acid methyl ester; MAME, mycolic acid methyl ester(s); MIC, minimal inhibitory concentration; TAG, triacylglycerol; TDM, trehalose dimycolate; TLC, thin layer chromatography; TMM, trehalose monomycolate; x_{I50}, inhibitor molar excess leading to 50% inhibition; FP, fluorophosphonate; DTNB, 5,5′-dithio-bis-(2-nitrobenzoic acid); DEP, *p*-nitrophenyl phosphate; TAMRA, carboxytetramethylrhodamine; ILI, intracellular lipid inclusion; r.m.s., root mean square; PDB, Protein Data Bank.

lates (10), whereas deletion of *fbpA* or *fbpB*, encoding Ag85A and Ag85B, respectively, led to reduced TDM levels (12–14), implying that although a level of functional redundancy exists *in vivo* between the three members, the contribution of each member is significant. The lack of double and triple knockout mutants might indicate that the loss of two or more Ag85 enzymes is detrimental to *M. tuberculosis* viability. An additional isoform, designated Ag85D or MPT51, has been characterized but found to be inactive due to the lack of catalytic elements required for mycolyltransferase activity (11, 15, 16). Ag85A/B/C share the same mycolic acid donor TMM, and their crystal structures present a highly conserved catalytic site, which further supports their similar enzymatic role (17–19).

Due to their importance in mycolic acid metabolism, the Ag85 enzymes have often been proposed as attractive targets for future chemotherapeutic developments against TB (9, 20–22). Because of their high structural conservation, it can be inferred that a single compound may inhibit all three enzymes of the complex at the same time and would make improbable the development of resistance to inhibitors, because resistant mutants would require the simultaneous acquisition of mutations in at least two *fbp* genes. In addition, because these proteins are secreted, targeting the Ag85 complex will minimize the effect of efflux mechanisms that may result in resistance phenotypes. Early inhibitors, such as trehalose analogs, were first designed as Ag85 inhibitors but were found to exhibit relatively poor activity on whole mycobacterial cells (9, 23). Another potentially selective fluorophosphonate α,α-D-trehalose inhibitor of the three antigen 85 enzymes has been reported to form a stable, covalent complex with the Ag85 enzyme following nucleophilic attack on the phosphorus atom of the catalytic Ser^{124} (24). In the same manner, the 2-amino-6-propyl-4,5,6,7-tetrahydro-1-benzothiophene-3-carbonitrile, designated I3-AG85, inhibits Ag85C, and exposure of *M. tuberculosis* to this compound was associated with reduced survival rates in broth medium and in infected primary macrophages. Moreover, I3-AG85 was active against a panel of multidrug-resistant/extensively drug-resistant strains, although it exhibited an MIC of 100 μM (25). By combining fragment-based drug discovery with early whole cell antibacterial screening, tetrahydro-1-benzothiophene analogs were discovered as potent Ag85C inhibitory molecules against drug-susceptible and drug-resistant *M. tuberculosis* strains (26). The selenazole compound ebselen (2-phenyl-1,2-benzisoselenazol-3(2H)-one) was found to inhibit the activity of Ag85C through an original mechanism by reacting with the conserved Cys^{209} residue located near the active site of the enzyme but not involved in the catalytic activity (27, 28). Ebselen was shown to directly impede the production of TDM and mycolylation of AG (27).

Recently, cyclipostins and cyclophostin (CyC), representing a new class of monocyclic enolphosph(on)ate compounds, have been discovered to act as powerful antitubercular agents affecting growth of *M. tuberculosis* both *in vitro* and in infected macrophages (29). Among the set of 27 CyC analogs previously evaluated against *M. tuberculosis* H37Rv, eight compounds exhibited potent anti-tubercular activities, particularly the cyclophostin analogs $CyC_{7\beta}$ and $CyC_{8\beta}$ as well as the cyclipostins-related molecule CyC_{17}. Whereas $CyC_{7\beta}$ exhibited a strong activity against extracellular and intracellular mycobacteria (MIC_{50} of 16.6 and 3.1 μM, respectively), $CyC_{8\beta}$ was mostly found to be active against intracellular bacteria (MIC_{50} $\sim$ 11.7 μM). In contrast, CyC_{17} was a potent inhibitor of *in vitro* growth (MIC_{50} $\sim$ 0.5 μM) but failed to show activity against intracellular bacilli (29). To identify the putative target(s) of the CyC inhibitors, an activity-based protein profiling approach was used based on TAMRA-FP and desthiobiotin-FP probes and mass spectrometry analyses. This led to the capture of several active serine/cysteine enzymes in a complex proteome before mass spectrometry identification, among which Ag85A (Rv3804c) and Ag85C (Rv0129c) were identified.

The present study was undertaken to further explore and validate, through a combination of biochemical and structural approaches, the specificity of inhibition of the Ag85 activity by the CyC analogs, to determine their mode of action and to describe how they affect the mycolic acid profile in *M. tuberculosis*.

Results

CyC analogs inhibit TDM biosynthesis and transfer of mycolic acids to arabinogalactan in M. tuberculosis

CyCs are a new class of compounds demonstrating potent antitubercular activity, presumably involving inhibition of the Ag85 activity (29). The chemical structures of the cyclophostin analogs $CyC_{7\beta}$ and $CyC_{8\beta}$ and the cyclipostins CyC_{17} used in this study are provided in Fig. 1*A*. To test whether treatment with these CyCs alters the mycolic acid composition of *M. tuberculosis* mc^26230, cultures were exposed to increasing concentrations of CyC_{17} or $CyC_{7\beta}$, the two inhibitors most active against extracellularly replicating *M. tuberculosis* (29), followed by metabolic labeling with sodium [2-^{14}C]acetate and lipid analysis. Extraction and separation of the total mycolic acid methyl esters (MAME) by thin layer chromatography (TLC) revealed that neither CyC_{17} nor $CyC_{7\beta}$ altered the *de novo* biosynthesis of mycolic acid (Fig. 1 (*B* and *C*), *left*). In contrast, separation of the apolar lipid fraction by TLC showed a dose-dependent decrease in TDM levels associated with a concomitant increase in the production of TMM, which is the natural substrate of the Ag85 proteins (Fig. 1 (*B* and *C*), *middle*). To address whether CyC treatment also impacts the cell wall-bound mycolic acids, radiolabeled mycolic acids were extracted from delipidated bacteria (30). The autoradiography/TLC analysis confirmed a dose-dependent inhibition of [2-^{14}C]acetate incorporation into all three forms of the AG-attached mycolic acids (α, methoxy, and keto), suggesting that treatment with CyC_{17} or $CyC_{7\beta}$ inhibits AG mycolylation at low concentrations (Fig. 1 (*B* and *C*), *right*). A quantitative analysis of these effects is provided in the corresponding graphs (Fig. 1, *B* and *C*).

Overall, this suggests that *in vivo* inhibition of the mycolyltransferase activity by the CyC compounds results in decreased formation of the virulence-associated TDM and reduced transfer of mycolic acids onto the essential cell wall AG.

Covalent inhibition of the Ag85C mycolyltransferase activity

All three members of the Ag85 complex, sharing between 65 and 75% sequence identity, have been shown to possess a serine

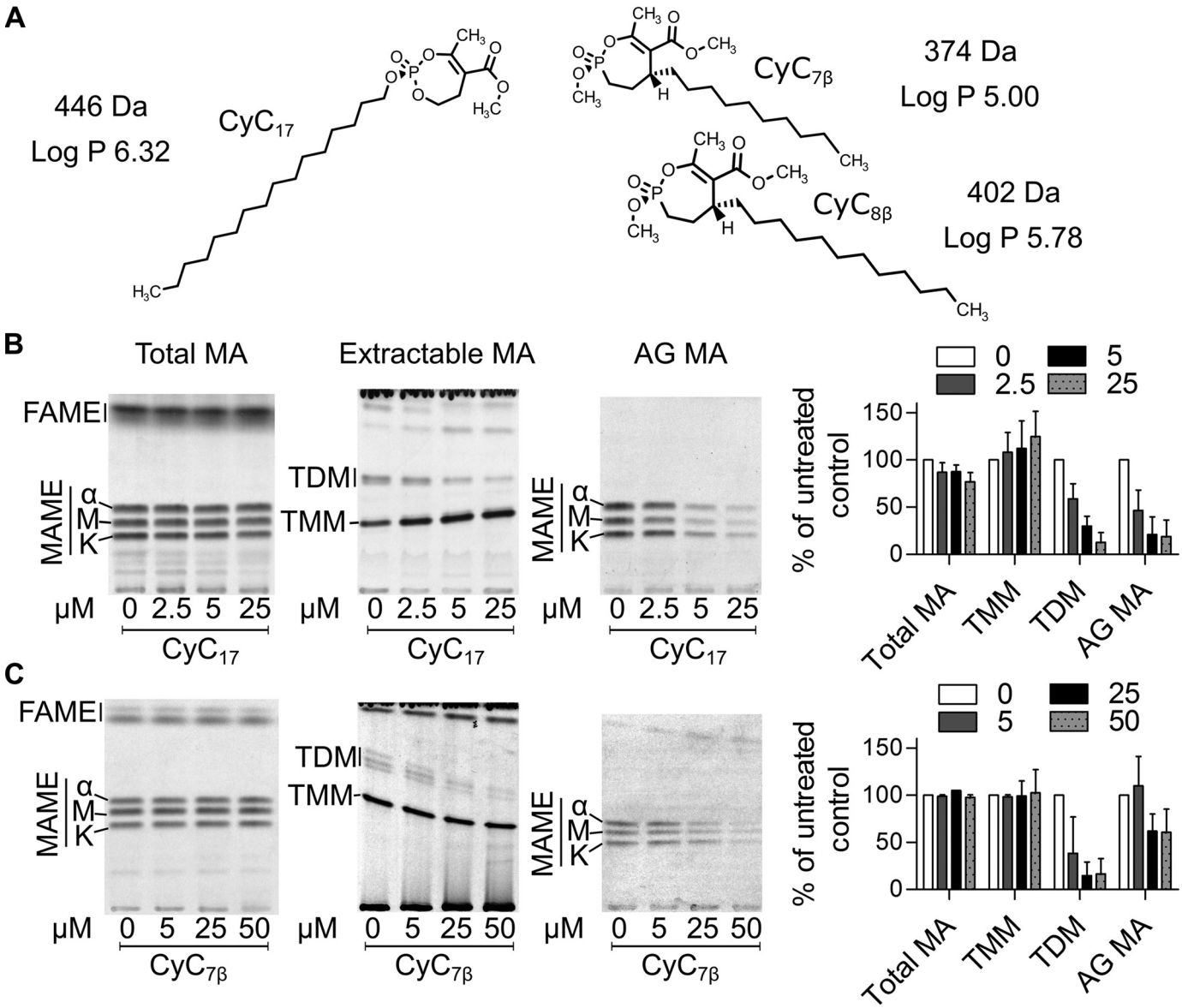

Figure 1. Ag85 complex mycolyltransferase activity is inhibited by CyC analogs *in vivo*. Exponentially growing *M. tuberculosis* mc^{2}6230 was incubated with increasing concentrations of CyC_{17} or $CyC_{7\beta}$ in 7H9$^{OADC/Tween\ 80}$ at 37 °C with agitation for 1 h. Subsequently, bacteria were labeled with sodium [2-^{14}C]acetate for 6 h at 37 °C with agitation. The cultures were split, and from the first volume were extracted the total methyl esters of mycolates (MAME) and fatty acids (FAME). From the second volume, apolar and polar lipid fractions were obtained before derivatization of arabinogalactan MAME. *A*, chemical structures of the CyC analogs used in this study. *B* and *C*, effect of CyC_{17} (*B*) or $CyC_{7\beta}$ (*C*) treatment on the mycolic acid profiles of *M. tuberculosis* mc^{2}6230. Equal counts (50,000 cpm) of MAME + FAME fraction were loaded on a TLC plate and resolved once using the solvent system hexane/ethyl acetate (95:5, v/v) run twice (*far left*). The apolar fraction was loaded (50,000 cpm), and TMM and TDM were visualized on a 1D TLC plate using the solvent system chloroform/methanol/water (40:8:1, v/v/v) (*middle left*). Equal volumes of arabinogalactan MAME fraction were loaded, and α, methoxy, and keto mycolic acids were visualized on a 1D TLC plate using the solvent system hexane/ethyl acetate (95:5, v/v) run twice (*middle right*). Densitometric analysis (*far right*) was performed on the TLCs shown in the left panels. *Histograms* and *error bars*, means and S.D. values calculated from at least two independent experiments.

hydrolase mycolyl esterase/transferase activity (17–19). To test the hypothesis that CyC analogs inhibit the activity of the three Ag85 members, we first cloned *Ag85C* (*fbpcC2*) into pET23b, and the recombinant protein was produced in *Escherichia coli*. The protein was then purified from lysates of *E. coli* by successive nickel-affinity, anion-exchange, and size-exclusion chromatography steps, leading to 3 mg of pure protein/liter of culture. Using a recently developed fluorescent assay based on resorufin butyrate as the acyl donor for Ag85C and trehalose as the acyl acceptor (27), we investigated whether $CyC_{7\beta}$, $CyC_{8\beta}$, and CyC_{17} inhibit the acyltransferase activity onto trehalose. In each case, a dose-dependent inhibition was observed with all three compounds, with $CyC_{8\beta}$ being the most efficient inhibitor (IC_{50} of 15 ± 5 μM), followed by $CyC_{7\beta}$ (IC_{50} of 43 ± 3 μM) and CyC_{17} (IC_{50} of 98 ± 6 μM) (Fig. 2*A*). Moreover, in terms of molar excess of inhibitor ($x_{150} = IC_{50}/[Ag85C]$) (31), all three CyCs react almost in stoichiometry with pure Ag85C, as judged by their respective x_{150} values of around 0.3, 0.8, and 1.8, respectively.

To address the inhibitory effect on the mycolyltransferase assay, Ag85C (55 μM) was next incubated for 30 min in its native form with 500 μM (*i.e.* enzyme/inhibitor molar ratio of 1:9) of each CyC compound. As expected, the complete loss of activity was confirmed by comparing the pretreated *versus* non-treated

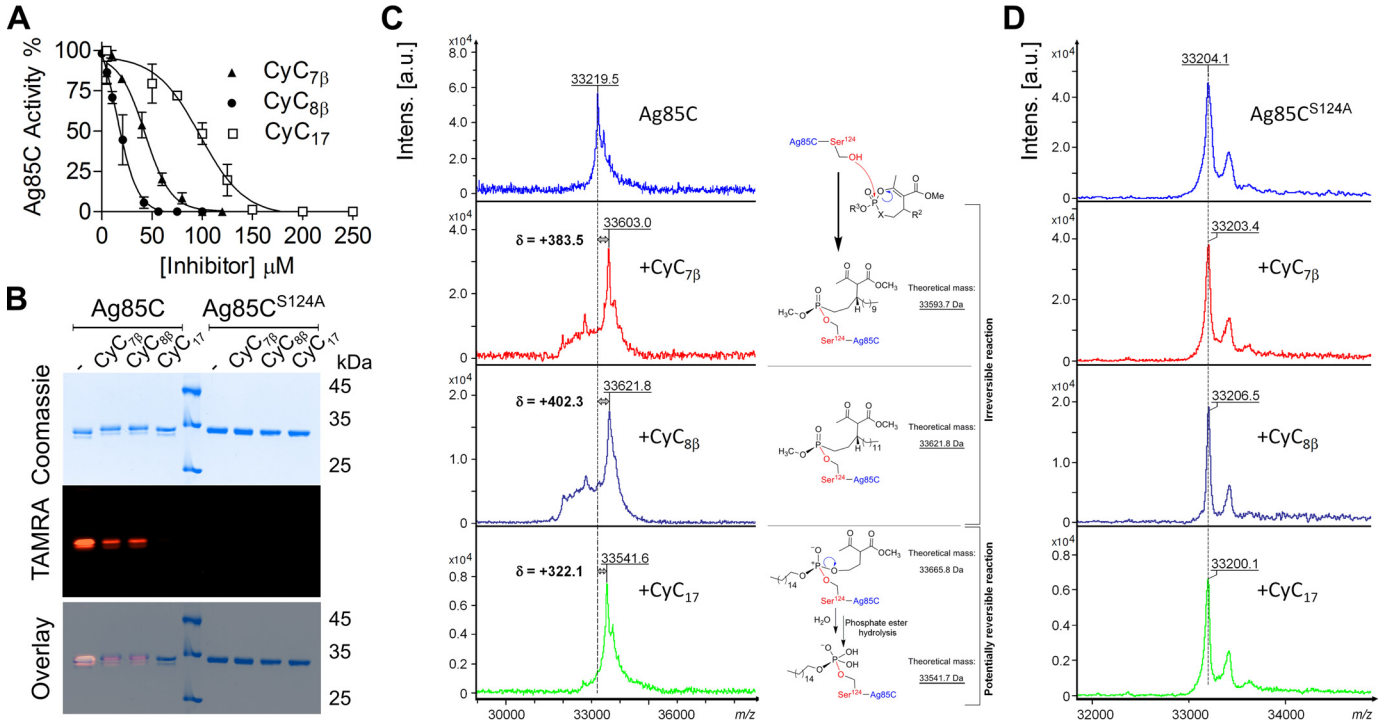

Figure 2. Inhibition of the Ag85C mycolyltransferase activity is mediated by the covalent binding of CyC analogs. *A*, the enzymatic activity of Ag85C was tested using a fluorescence-based assay in the presence of different concentrations of $CyC_{7\beta}$, $CyC_{8\beta}$, and CyC_{17}. The inhibitory effect was determined at the maximum rate of the reaction. *Error bars*, S.D. calculated from three independent experiments. *Curves* for $CyC_{7\beta}$, $CyC_{8\beta}$, and CyC_{17} were fitted using the EC_{50} shift non-linear regression model in GraphPad Prism with R^2 values of 0.9675, 0.9508, and 0.9415, respectively. *B*, equal amounts of either Ag85C or $Ag85C^{S124A}$ were pretreated with $CyC_{7\beta}$, $CyC_{8\beta}$, and CyC_{17}; incubated with TAMRA-FP, separated by SDS-PAGE; and visualized by Coomassie Blue staining (*top*) or in-gel fluorescence visualization (*middle*). The *merged image* is shown at the *bottom*. TAMRA labeling of Ag85C is prevented by the covalent binding of the CyC analogs to the catalytic Ser^{124}. No TAMRA-FP labeling is seen for the $Ag85C^{S124A}$ variant, confirming Ser^{124} as the TAMRA-binding site. *C* and *D*, global mass modification of Ag85C (*C*) and $Ag85C^{S124A}$ (*D*) preincubated with $CyC_{7\beta}$, $CyC_{8\beta}$, and CyC_{17} as determined using an Ultraflex III mass spectrometer (Bruker Daltonics) in linear mode with the LP_66 kDa method. The mechanism of action of the phosphonates $CyC_{7\beta}$ and $CyC_{8\beta}$ and of the phosphate analog CyC_{17} based on mass spectrometry analyses is illustrated in *C*. *a.u.*, arbitrary units.

Ag85C. All three Ag85C-CyC adducts were treated with 10 μM TAMRA-FP fluorescent probe, known to bind to serine enzymes (32), for 1 h, and equal amounts of proteins were separated by SDS-PAGE and visualized by Coomassie staining (Fig. 2*B*, *top*) or in-gel fluorescence for TAMRA detection (Fig. 2*B*, *middle*). Pretreatment with either $CyC_{7\beta}$ or $CyC_{8\beta}$ resulted in a significant loss in fluorescence intensity (about 75%) as compared with the non-treated protein, whereas incubation with CyC_{17} abrogated TAMRA labeling. This suggests that reaction with the TAMRA probe is strongly impaired in the Ag85C-CyC adducts, resulting in a decrease/loss of fluorescence emission. To determine the implication of the conserved catalytic Ser^{124} in Ag85C in TAMRA labeling, this residue was replaced by an Ala residue, and the mutated protein was purified (Fig. 2*B*, *top*). Exposure of TAMRA to $Ag85C^{S124A}$ failed to produce a fluorescence signal (Fig. 2*B*, *middle*), indicating that the catalytic Ser^{124} is required for binding of the probe. As expected, no fluorescence emission was observed when pretreating the mutated protein with the CyC analogs (Fig. 2*B*, *bottom*).

MALDI-TOF mass spectrometry was further used to study the (covalent) nature of the inhibition. Mass increments of +383.5 and +402.3 Da in the presence of $CyC_{7\beta}$ and $CyC_{8\beta}$, respectively, were observed within the global mass of treated Ag85C as compared with the global mass of untreated Ag85C (Fig. 2*C*). In contrast, no changes in the global mass were observed with the inactive $Ag85C^{S124A}$ protein (Fig. 2*D*). These data thus support the formation of a covalent Ag85C-CyC complex, as the reaction between the catalytic Ser^{124} and either $CyC_{7\beta}$ or $CyC_{8\beta}$ is expected to yield mass increases of +374.2 or +402.25 Da, respectively. Moreover, such results are consistent with the known and irreversible classical mechanism of action of phosphonate compounds, as demonstrated using pure mycobacterial lipolytic enzymes (31).

With respect to CyC_{17}, the observed 322.1-Da mass shift increment was 124.18 Da lower than its expected theoretical molecular mass of 446.28 Da (Fig. 2*C*). This size difference may arise from the specific chemical properties of phosphate (*i.e.* CyC_{17}) *versus* phosphonate (*i.e.* $CyC_{7\beta}$ and $CyC_{8\beta}$) chemical groups. In all cases, the nucleophilic attack of catalytic Ser^{124} at the phosphorus center induces ring opening. However, the reaction with CyC_{17} is very likely to form a new phosphate triester, which in turn becomes susceptible to hydrolysis. From these findings, it can be inferred that once the CyC_{17}-Ser^{124} adduct is formed, it becomes rapidly hydrolyzed in the presence of water, resulting in the cleavage and release of the methyl 2-acetyl-4-hydroxybutyrate (*i.e.* 124.1 Da), accounting exactly for the molecular mass discrepancy observed experimentally (Fig. 2*C*).

Taken together, these findings conclusively indicate that Ag85C is covalently modified by CyC analogs, leading to the inhibition of the mycolyltransferase activity and thus supporting the *in vivo* alteration of the mycolic acid pattern by these compounds.

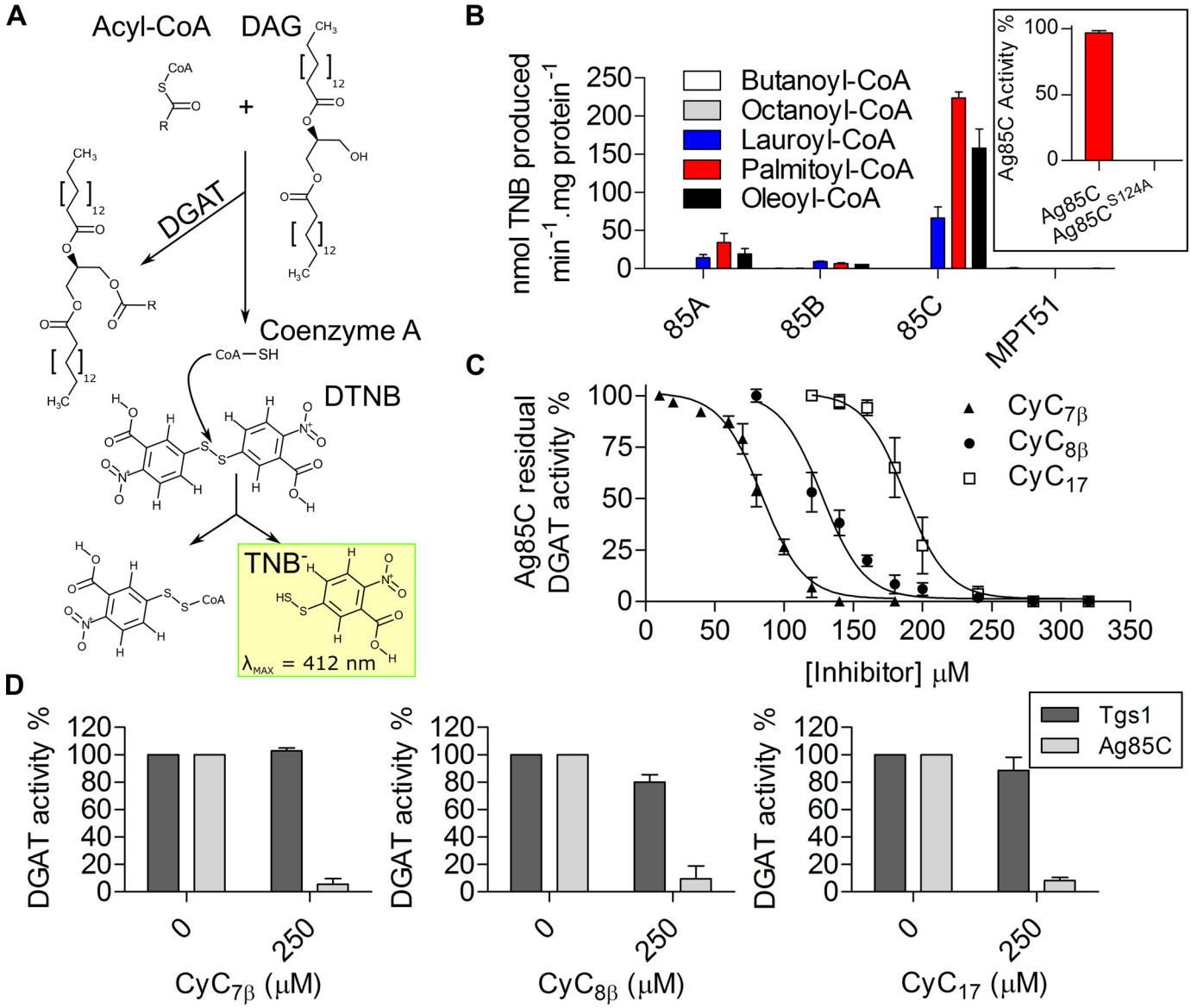

Figure 3. DGAT activity of the antigen 85 complex and inhibition by CyC analogs. *A*, chemical reaction occurring while determining the DGAT activity. DTNB reacts with the free-thiol group coming from the release of SH-CoA during the formation of TAG from 1,2-dipalmitoylglycerol (*DAG*) and a molecule of acyl-CoA. *B*, comparison of the DGAT activity of Ag85A, Ag85B, Ag85C, and MPT51. Enzymatic activity was determined by the colorimetry-based assay illustrated in *A*. *Inset*, activity of the wildtype and S124A Ag85C proteins using palmitoyl-CoA (*C16*) as acyl donor molecule. *Error bars*, S.D. calculated from three independent experiments. *C*, inhibitory effect of CyC analogs on Ag85C DGAT activity. Inhibition was performed with increasing concentrations of $CyC_{7\beta}$, $CyC_{8\beta}$, and CyC_{17} using the colorimetry-based assay illustrated in *A*. The inhibitory effect was determined after 1 h of reaction. *Error bars*, S.D. calculated from three independent experiments. Curves for $CyC_{7\beta}$, $CyC_{8\beta}$, and CyC_{17} were fitted using the EC_{50} shift non-linear regression model on GraphPad with R^2 values of 0.9755, 0.9641, and 0.9422, respectively. *D*, comparison of the DGAT activity of Ag85C and Tgs1 in the absence or presence of $CyC_{7\beta}$, $CyC_{8\beta}$, and CyC_{17}.

Ag85A, -85B, and -85C express DGAT activity

Although the mycolyltransferase activity of the Ag85 complex has been established for a long time (8, 9), more recent work suggested that Ag85A mediates the transesterification of diacylglycerol using long-chain acyl-CoA to produce triglycerides (TAG), which act as storage compounds for energy and carbon (33). Ag85A contains the same catalytic triad as Ag85C or Ag85B, formed by residues Ser^{126}, His^{262}, and Glu^{230}, and possesses a deep substrate-binding groove near the active-site serine, suggesting that Ag85B and Ag85C, similarly to Ag85A, may also express diacylglycerol acyltransferase (DGAT) activity. To test this hypothesis, all of the genes were cloned into pET23b, and the recombinant proteins were produced in *E. coli* and purified from lysates by successive nickel-affinity, anion-exchange, and size-exclusion chromatography steps. Because Ag85B was poorly expressed in *E. coli*, a synthetic gene was produced by replacing low-usage codons with high-usage codons, as reported previously (34) and subsequently cloned into pET23a. All three proteins were assayed for DGAT activity in the presence of acyl-CoA with various chain lengths (from C4 to C18) as acyl donors and 1,2-dipalmitoyl-*sn*-glycerol (1,2-dipalmitin) as the acyl acceptor, as illustrated in Fig. 3*A*. Transesterification in the presence of 5,5′-dithio-bis-(2-nitrobenzoic acid) (DTNB) leads to the formation of TNB, which can readily be measured at 412 nm (33, 35). In agreement with previous findings, Ag85A was found to express DGAT activity, but such

an activity was only detected with C12-C18 acyl-CoAs (Fig. 3*B*). Whereas Ag85B demonstrated lower activity than Ag85A, Ag85C showed the highest activity, which was optimal in the presence of C16-CoA. No activity was detected with the C4- or C8-containing acyl chains. We also expressed and purified the Ag85 complex-related MPT51 (FbpC1) protein, which possesses an overall structure similar to that of the Ag85 complex members but is defective in the catalytic elements required for mycolyltransferase activity (11, 16). As anticipated, MPT51 failed to express any DGAT activity, suggesting that residues important for mycolyltransferase activity are also key players in the DGAT activity, as proposed earlier for the Ser^{126} in Ag85A (33). Purified $Ag85C^{S124A}$ was next assayed with various acyl-CoA substrates, and, as shown in Fig. 3*B* (*inset*), the DGAT activity was abrogated in the mutant protein, implying that Ser^{124} plays a critical role in the enzymatic reaction.

Overall, these data extend insights from previous findings and indicate that all three members of the Ag85 complex express DGAT activity, with Ag85C exhibiting the most pronounced activity. This suggests that Ag85C may also make an important contribution in TAG synthesis in *M. tuberculosis*.

CyC analogs inhibit the in vitro DGAT activity of Ag85C but not of Tgs1

The above-mentioned results prompted us to investigate whether CyC analogs alter the DGAT activity of Ag85C. This was achieved by incubating the purified enzyme in the presence of increasing concentrations of $CyC_{7\beta}$, $CyC_{8\beta}$, and CyC_{17} using the colorimetric activity assay described in the legend to Fig. 3*A*. As expected from the previous results on the inhibition of mycolyltransferase activity, a dose-dependent inhibition of the DGAT activity with all three compounds was also observed (Fig. 3*C*). $CyC_{7\beta}$ appeared as the most potent inhibitor, with an IC_{50} value of 85 ± 2 μM (*i.e.* $x_{I50} = 2.8$), followed by $CyC_{8\beta}$ and CyC_{17} exhibiting IC_{50} values of 121 ± 4 μM (*i.e.* $x_{I50} = 4.0$) and 187 ± 3 μM (*i.e.* $x_{I50} = 6.2$), respectively.

Because the TAG synthase *tgs1* in *M. tuberculosis* and *Mycobacterium abscessus* has been reported as the major contributor of TAG accumulation in the form of intracellular lipid inclusions (ILIs) in these two species (35, 36), we addressed whether the DGAT activity of Tgs1 may also be targeted by the CyC analogs. Tgs1 from *M. tuberculosis* (Rv3130c) was expressed and purified from *E. coli* and subsequently used in a DGAT assay in the absence or presence of either $CyC_{7\beta}$, $CyC_{8\beta}$, or CyC_{17} (Fig. 3*D*). Whereas the activity of Tgs1 remained intact even in the presence of a 250 μM concentration of each compound, the DGAT activity of Ag85C assayed in the same conditions was almost abrogated, suggesting that Tgs1 activity is not impacted by CyC treatment.

These results indicate that CyC analogs specifically inhibit the DGAT activity of Ag85C but not of Tgs1 *in vitro*, in agreement with the fact that members of the Tgs family were not identified in our original proteomic profiling study (29).

Overexpressing Ag85C in M. tuberculosis is associated with reduced inhibition of TAG production by CyC_{17}

That Ag85C expresses the highest DGAT activity among the three members of the Ag85 complex prompted us to address whether overexpression of Ag85C in *M. tuberculosis* affects the TAG content. *M. tuberculosis* was first transformed with either pMV261-Ag85C or pMV261-$Ag85C^{S124A}$. Overexpression of either the wildtype or the catalytically dead proteins was checked by quantitative real-time PCR (Fig. 4*A*, *left*) and by immunoblotting using two different monoclonal antibodies and purified Ag85A, -B, and -C as positive controls (Fig. 4*A*, *right*). The 17/4 monoclonal antibody recognizes a well-conserved epitope present in Ag85A and Ag85B but not in Ag85C (37). In contrast, the 32/15 antibody revealed all three antigens and the presence of more pronounced bands in the pMV261-Ag85C and pMV261-$Ag85C^{S124A}$ lysates, which, by comparison with the 17/4 blot, could clearly be attributed to Ag85C (Fig. 4*B*, *right*). This indicates that both Ag85C variants were overproduced at comparable transcriptional and translational levels and allowed us to investigate whether this may affect the intracellular TAG content of *M. tuberculosis* (38). TAGs are often stored in the form of ILIs, which can be visualized by staining with Nile Red (39, 40). As shown in Fig. 4*B* (*left*), although a punctiform labeling corresponding to ILIs is observed in the control strain carrying the empty pMV261, Nile Red straining was much more pronounced in the strain overproducing Ag85C, and the effect returned to control levels in the strain harboring pMV261-$Ag85C^{S124A}$. Quantification of the fluorescence intensity over the entire length of the individual bacilli from each strain clearly indicates that large and numerous ILIs were present in the Ag85C-overexpressing strain, as compared with the control and $Ag85C^{S124A}$ strains (Fig. 4*B*, *right*).

To check whether enhanced ILI formation coincided with increased *de novo* biosynthesis of TAG, metabolic labeling of *M. tuberculosis* cultures with sodium [2-^{14}C]acetate was performed, followed by extraction and separation of the apolar lipid fraction by TLC. In the absence of CyC treatment, the strain carrying pMV261-Ag85C produced moderately higher amounts of TAGs than the control strain containing the empty pMV261 or the strain overexpressing $Ag85C^{S124A}$ (Fig. 4*C*, *left*), supporting the *in vivo* contribution of Ag85C in TAG production. Importantly, exposure to CyC_{17} inhibited TAG biosynthesis in a dose-dependent manner in the control strain, thus implying that the *de novo* biosynthesis of TAG is also targeted by CyC_{17} (Fig. 4*C*). In addition, a less pronounced decrease in TAG production occurred in the strain overexpressing Ag85C as compared with the control strain, presumably because of the inherent capacity of this strain to synthesize more TAG that partially overcomes CyC_{17} inhibition (Fig. 4*C*). Collectively, these results suggest that TAG production in *M. tuberculosis* is inhibited by CyC_{17} and that this is dependent upon Ag85C DGAT activity.

Crystal structure of the $CyC_{8\beta}$-bound Ag85C

To gain insight into the mode of action of the CyC compounds, crystallization studies of Ag85C were undertaken in the presence of the three CyC inhibitors. However, diffracting crystals were only obtained with $CyC_{8\beta}$ for which the X-ray structure of Ag85C bound to $CyC_{8\beta}$ was solved at a resolution of 1.8 Å (Table 1). The asymmetric unit contains two molecules of Ag85C (Fig. 5*A*). Residues 6–282 and 8–282 for each subunit

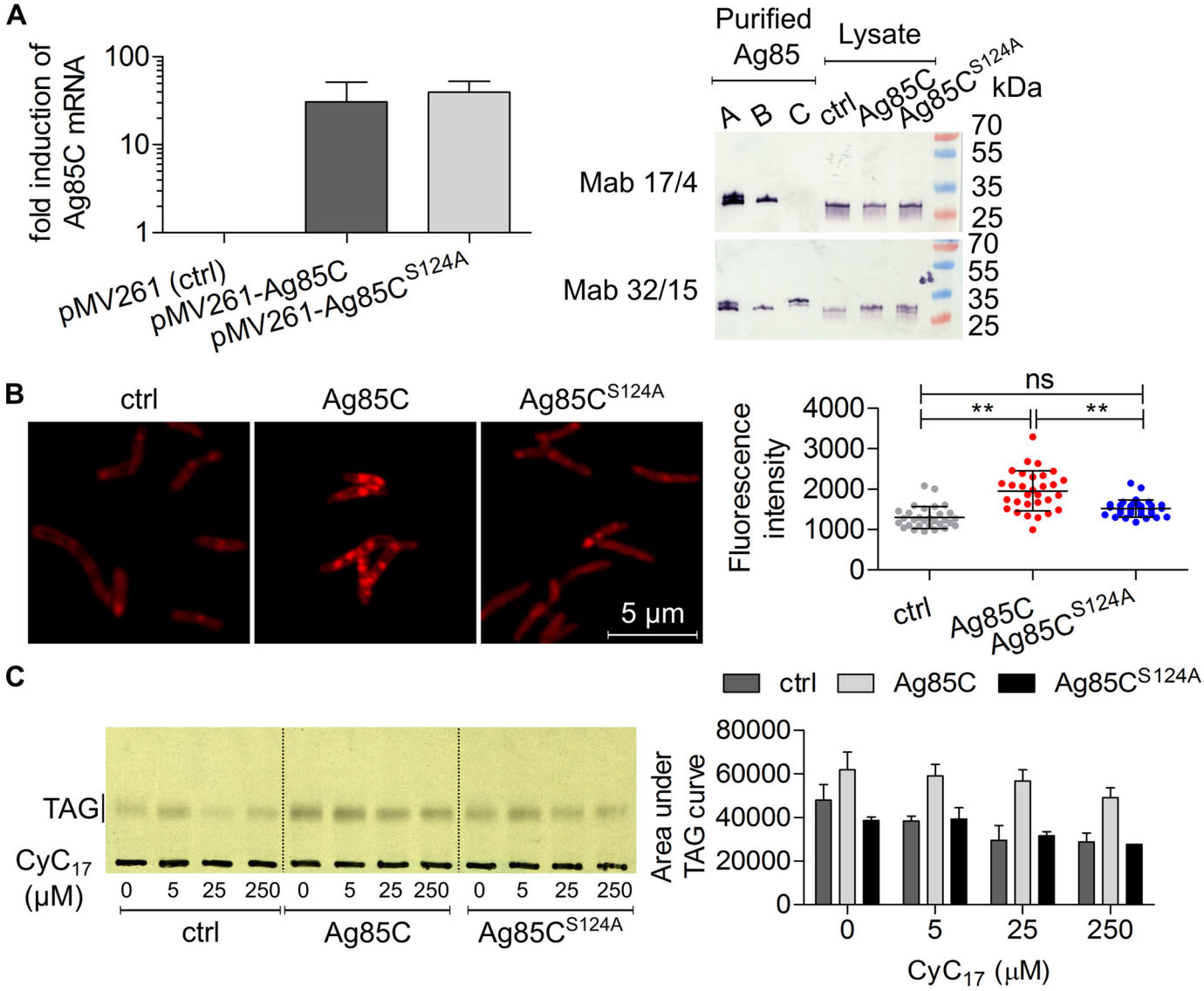

Figure 4. Biosynthesis of TAG in *M. tuberculosis* is inhibited by CyC_{17} and is dependent upon Ag85C expression. *A*, quantitative real-time PCR analysis showing the -fold increase in the Ag85C transcripts in *M. tuberculosis* mc^{2}6230 containing either pMV261 (*ctrl*), pMV261-Ag85C, or pMV261-Ag85C^{S124A} (*left*). Western blotting using the 32/15 and 17/4 monoclonal antibodies probed against purified Ag85A/B/C and crude lysates of *M. tuberculosis* mc^{2}6230 containing either pMV261, pMV261-Ag85C, or pMV261-Ag85C^{S124A} (*right*). *B*, Nile Red staining of *M. tuberculosis* strains growing exponentially (*left*) with the corresponding fluorescence quantification (*right*). Fluorescence quantification was performed on 30 bacilli of each group. Shown are the mean fluorescence and S.D. values. Means were compared by the two-tailed Mann–Whitney test. *ns*, non-significant; **, $p < 0.01$. Results shown are representative of two independent experiments. *C*, cultures were exposed to increasing concentrations of CyC_{17} in 7H9$^{OADC/Tween\ 80}$ and labeled with sodium [2-^{14}C]acetate for 4 h at 37 °C with agitation. The apolar fraction was extracted to analyze *de novo* synthesis of TAG. Equal counts (50,000 cpm) of apolar fraction were loaded, and TAG was visualized on a 1D TLC plate using the solvent system petroleum ether/diethyl ether (90:10, v/v) (*left*). *Right*, densitometric analysis of TLCs. *Histograms* and *error bars*, means and S.D. values calculated from four independent experiments.

could be built, implying that the last 14 residues as well as the polyhistidine tag in the C terminus were not modeled. The structure of Ag85C has been extensively reported (17). In brief, the protein adopts a typical α/β hydrolase fold made of a central β-sheet surrounded by α-helices. The two monomers are nearly identical, as their superposition over 274 residues gives an r.m.s. deviation of 0.24 Å. However, whereas a clear electron density could be seen for the entire structure of $CyC_{8\beta}$ in one monomer, this was only the case for the headgroup of the second molecule (Fig. 5*B*). It is noteworthy that the extra but non-interpretable electron density (Fig. 5*B*) in the vicinity of $CyC_{8\beta}$, observed in all data sets collected from either co-crystallization or soaking experiments and in various crystallization conditions (data not shown), appears as a possible molecule interacting with Phe^{150} and could be seen in both monomers. As Phe^{150} was shown to be involved in stacking of the lipid chain of octylglucoside in the Ag85C-octylglucoside crystal structure (PDB entry 1VA5 (19)), we tried to place the acyl chain of $CyC_{8\beta}$ in this extra electron density, but refinement of this alternate conformation of $CyC_{8\beta}$ did not converge. Therefore, further modeling of this electron density blob was not pursued. Although $CyC_{8\beta}$ has clearly reacted, as evidenced by the presence of an opened ring and the MALDI-TOF data, no covalent bond between the catalytic Ser^{124} residue and the phosphonate group of $CyC_{8\beta}$ was observed (Fig. 5, *B* and *D*). Therefore, $CyC_{8\beta}$ was modeled in an opened conformation (Fig. 5, *B* and *D*). $CyC_{8\beta}$

Table 1
Data collection and refinement statistics

Data collection statistics	
Beamline	ESRF-ID23.1
Wavelength (Å)	0.972
Resolution range (Å)	48.09–1.8 (1.86–1.8)[a]
Space group	$P\,2_1\,2_1\,2_1$
Unit cell	
Å	67.39, 75.77, 137.32
Degrees	90, 90, 90
Total reflections	528,844 (50,342)
Unique reflections	65,871 (6486)
Completeness (%)	99.92 (99.85)
Mean $I/\sigma(I)$	16.66 (2.24)
Wilson *B*-factor (Å^2)	24.34
R_{meas}	0.0968 (1.049)
Refinement statistics	
Reflections used in refinement	65,862 (6486)
R_{work}	0.151 (0.232)
R_{free}	0.175 (0.269)
No. of non-hydrogen atoms	4895
Macromolecules	4308
Ligands	54
Solvent	533
No. of r.m.s. deviations	
Bonds (Å)	0.006
Angles (degrees)	0.84
Ramachandran favored (%)	96.7
Ramachandran allowed (%)	3.3
Ramachandran outliers (%)	0.00
Rotamer outliers (%)	1.12
Clashscore	1.07
Average *B*-factor	29.13
Macromolecules	27.22
Ligands	50.05
Solvent	42.43
PDB accession number	5OCJ

[a] The values in parenthesis are for the highest-resolution shell.

interacts through residues at the entrance of the Ag85C active site (Fig. 5, *C* and *D*). The polar head of $CyC_{8\beta}$ is recognized through hydrogen bonds with the catalytic Ser^{124} side chain as well as with the main chain of Leu^{40} and the Asp^{38} side chain via two water molecules. The Arg^{41} side chain completes the interaction with the headgroup of $CyC_{8\beta}$ by van der Waals interaction (Fig. 5*D*). The long aliphatic chain of $CyC_{8\beta}$ is stabilized by hydrophobic interactions involving the Ile^{222}, Pro^{223}, Phe^{226}, and Leu^{227} side chains (Fig. 5*D*). The distance between the phosphate of $CyC_{8\beta}$ and Ser^{124} of 3.6 Å clearly attests that in this crystal, the ligand is not covalently bound. Importantly, this loss of covalent binding was observed in multiple data sets collected, obtained either by soaking or co-crystallization experiments. However, the lack of covalent binding in the crystal structure does not rule out the well-known covalent inhibitory mechanism of the CyC analogs supported by MALDI-TOF mass spectrometry analyses (Fig. 2, *C* and *D*).

Furthermore, the polar headgroup of $CyC_{8\beta}$ is located where trehalose, the natural substrate of the Ag85 proteins, binds, as seen in the crystal of the trehalose-bound structure of Ag85B (PDB entry 1F0P (18)) (Fig. 6*A*). Interestingly, the fatty acyl chain of $CyC_{8\beta}$ is placed in a very hydrophobic cavity that was proposed to be part of the TDM/TMM fatty chain recognition site (17). In addition, structural comparison indicated that the important residues in Ag85C interacting with $CyC_{8\beta}$ are fully conserved in Ag85B and Ag85A (Fig. 6*B*), strongly suggesting that $CyC_{8\beta}$, and presumably all of the other CyC analogs, may inhibit the three members of the Ag85 complex.

Discussion

Toward the generation of new lead compounds with unexplored modes of action in *M. tuberculosis*, the CyC analogs were initially designed to inhibit mycobacterial lipases (31). In particular, by covalently binding to the catalytic serine, they fully inactivated the monoacylglycerol lipase Rv0183 and the triacylglycerol lipase LipY from *M. tuberculosis* but not the mammalian gastric and pancreatic lipases (31). Subsequent biochemical studies involving the selective labeling and enrichment of captured enzymes using appropriate fluorophosphonate probes in combination with CyC_{17} resulted in the identification of 23 potential target lipolytic enzymes, all of which comprise catalytic serine or cysteine residues (29). Because they are multitarget-inhibitory compounds in mycobacteria, the use of CyC analogs could prevent the selection of drug resistance mechanisms. In addition, the lack of cytotoxicity in human cells (29) makes them attractive hits to be further evaluated.

Herein, we provide compelling evidence that at least some of the CyC analogs primarily act by inhibition of the Ag85 complex, resulting in decreased TDM formation and reduced mycolylation of AG, an essential polymer of the mycobacterial cell wall. Although one cannot rule out the possibility that the killing effect of the CyC on *M. tuberculosis* results from the simultaneous and net effect on multiple physiological targets, the inhibition of TMM and AG mycolylation is very likely to represent the major cause of growth inhibition of *M. tuberculosis*, at least in *in vitro* growing cultures. We demonstrate here that all three Ag85 members express DGAT activity *in vitro*, with Ag85C being the most active, thereby extending previous work reporting the DGAT activity of Ag85A (33). Importantly, the S124A site-directed mutation of the active site of Ag85C proved that this residue is involved in the DGAT activity of this enzyme and TAG synthesis. Although the synthesis of TAG relies on the presence of multiple TAG synthases, such as the well-characterized Tgs1 (Rv3130c) (36), our work extends the growing list of enzymes displaying DGAT activity in *M. tuberculosis*. The Ag85 proteins do not belong to the known DGAT families and do not possess the characteristic conserved heptapeptide acyltransferase motif of the mycobacterial Tgs enzymes involved in TAG biosynthesis (35, 41). Nevertheless, the DGAT activity of Ag85C, similarly to Ag85A (33), includes two consecutive reactions, the fatty acyl-CoA hydrolysis (thioesterification) and the subsequent transfer of the acyl chain to the diacylglycerol (transesterification). Overexpressing Ag85C in *M. tuberculosis* was correlated with an increase in *de novo* TAG production and formation of lipid storage inclusions. These findings establish for the first time a connection between cell wall and TAG biosynthesis by Ag85C and expand our understanding of this important enzyme in the physiology of *M. tuberculosis.* However, a direct implication of the DGAT activity of Ag85C in pathogenesis and persistence of *M. tuberculosis* requires further studies. In addition, under conditions where Ag85C is overexpressed, *M. tuberculosis* was more refractory to TAG inhibition by CyC_{17}, further emphasizing the yet unexpected contribution of Ag85C as a player in TAG biosynthesis. Inhibition of the DGAT activity of Ag85C, and therefore TAG inhibition, by the CyC compounds is very unlikely to

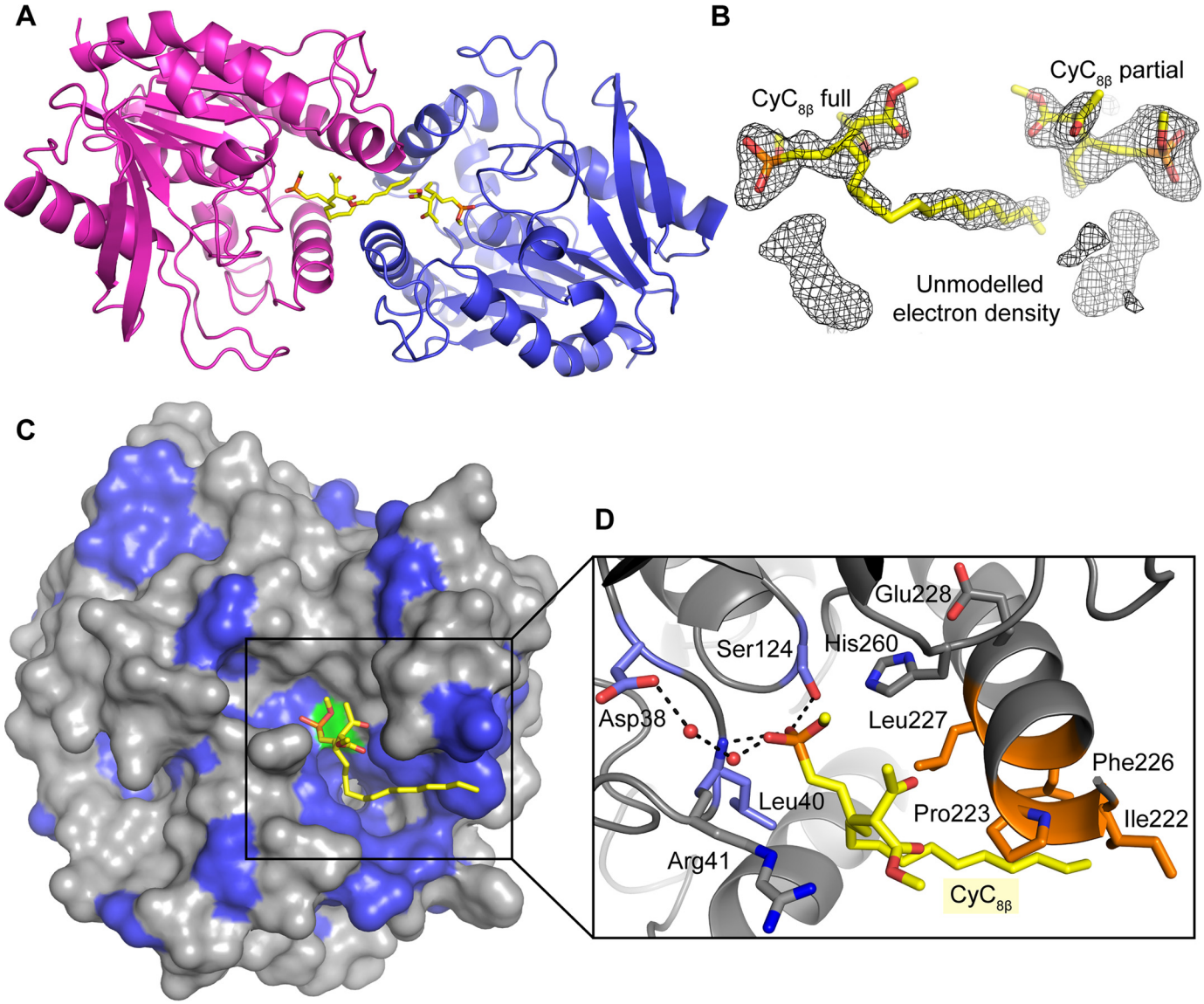

Figure 5. Structural basis for Ag85C inhibition by $CyC_{8\beta}$. *A*, crystal structure of Ag85C in complex with $CyC_{8\beta}$. The figure displays the overall asymmetric unit with the two monomers represented as *blue* and *magenta schematics*. $CyC_{8\beta}$ is shown as *sticks* and *colored* in *yellow*. *B*, simulated annealing $F_o - F_c$ OMIT map contoured at 3σ attesting to the presence of two $CyC_{8\beta}$ that could be entirely modeled for one molecule and partially for the second one. The map also reveals the presence of an extra, but non-interpretable, electron density in the vicinity of the $CyC_{8\beta}$ molecule. *C*, surface representation of the Ag85C structure bound to $CyC_{8\beta}$. The hydrophobic residues are *colored* in *blue*, and the catalytic Ser^{124} is shown in *green*. *D*, $CyC_{8\beta}$ binding site. Ag85C residues involved in $CyC_{8\beta}$ recognition are displayed as *blue sticks* for those involved in hydrogen bond (*black dashes*) formation. Residues in *orange* are involved in hydrophobic interactions with the acyl chain of $CyC_{8\beta}$, and Arg^{41} in *gray* contributes to the recognition of the $CyC_{8\beta}$ headgroup by van der Waals interaction. Ser^{124}, Glu^{228}, and His^{260} form the catalytic triad. *Red spheres*, water molecules.

participate in growth inhibition of *M. tuberculosis in vitro*, but it may have important consequences for *in vivo* survival and/or for maintaining the bacilli in a non-replicating growth phase, such as in foamy macrophages in which *M. tuberculosis* is able to hydrolyze the host-derived TAGs from lipid bodies to fatty acids, which are then reprocessed as TAGs and stored within ILIs (42, 43). In these subcellular structures, TAGs represent the primary storage source of carbon and energy, allowing the bacteria to survive in a non-replicating state and to persist inside these foamy cells, which usually line the necrotic centers of tubercle granulomas and have been proposed to be the intracellular niche of *M. tuberculosis* during latent infection (42). Although this requires further exploration, inhibiting the DGAT activity of Ag85C may help in designing new classes of molecules that restrict entry of *M. tuberculosis* into dormancy, a strategy that would overcome mycobacterial persistence and prolonged chronic infections.

Biochemical studies involving the TAMRA-FP probe that binds to serine hydrolases along with mass spectrometry and structural analyses indicate that, in addition to covalently binding to the catalytic Ser^{124}, the CyC analogs could also be competing with the binding of Ag85 substrate (*i.e.* the trehalose and the acyl chain moieties of TMM). As the Ag85 complex members share similar substrate specificities, our results suggest that CyC analogs could target not only Ag85C but also Ag85B and Ag85A, an assertion reinforced by the fact that Ag85A was also identified as a potential target in the original proteomic screen approach (29). Comparison of the three structures

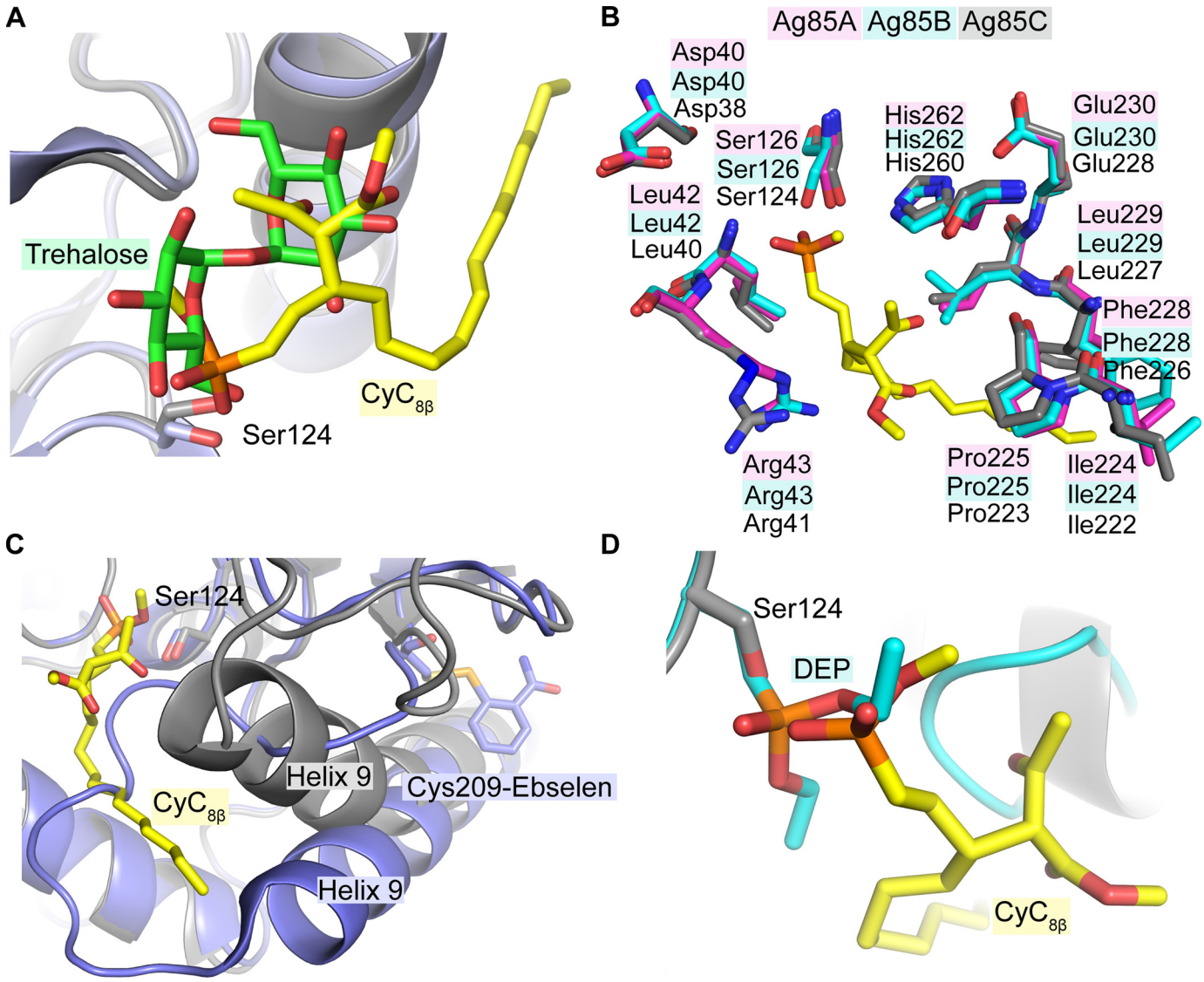

Figure 6. Mode of inhibition of the Ag85 complex by $CyC_{8\beta}$. *A*, superposition of the Ag85B-trehalose (PDB code 1F0P, *blue*) and Ag85C-$CyC_{8\beta}$ (*gray*) crystal structures. The headgroup of $CyC_{8\beta}$ (*yellow*) occupies the same site as trehalose (*green*). *B*, Ag85C residues (*gray*) involved in the recognition of $CyC_{8\beta}$ are all strictly conserved in Ag85B (*cyan*) and Ag85A (*magenta*). *C*, superposition of the Ag85C-ebselen (PDB code 4QDU; *blue*) and Ag85C-$CyC_{8\beta}$ (*gray*) crystal structures. $CyC_{8\beta}$ binds far away from the ebselen-binding site and does not trigger structural rearrangement of helix α9. *D*, superposition of the Ag85C-DEP (PDB code 1DQY; *cyan*) and Ag85C-$CyC_{8\beta}$ (*gray*) crystal structures. $CyC_{8\beta}$ presents a similar mode of inhibition as DEP (*cyan stick*), a nonspecific σ/β hydrolase inhibitor.

strongly supports this hypothesis, as residues contacting $CyC_{8\beta}$ in Ag85C are strictly conserved in Ag85A and Ag85B. This is of interest, as the inhibitor I3-AG85 binding to the active site of Ag85C exhibits only strict specificity toward Ag85C and does not bind Ag85A and -B (25). Moreover, given their low x_{150} values, the three CyC compounds are able to act in near stoichiometry and alter both the mycolyltransferase and DGAT activities of Ag85C. It is noteworthy that, among the three CyCs investigated, the phosphate CyC_{17}, which appears as the best inhibitor against extracellular *M. tuberculosis*, was the least efficient when assayed on pure recombinant enzyme. However, when assayed on living bacteria, CyC_{17} clearly affected TDM synthesis and mycolylation of AG. The differences in activity with $CyC_{7\beta}$ and $CyC_{8\beta}$ may be related to the chemical properties of the phosphate *versus* phosphonate chemical groups. On the other hand, despite their high activity, phosphate inhibitors can be subjected to hydrolysis, rendering their covalent binding potentially reversible, as shown here in the case of the CyC_{17}-Ser^{124} adduct (29). Interestingly, using a chemical proteomic approach, the EZ120 β-lactone compound exhibiting strong antitubercular activity and resembling an electrophilic mimic of mycolic acids was recently found to block several serine hydrolases essential for the mycomembrane biosynthesis (44). The polyketide synthase Pks13, whose β-keto mycolate is transferred onto trehalose and reduced to yield TMM, as well as Ag85A were identified as primary targets of EZ120. However, whether this β-lactone acts similarly to the CyC inhibitors in Ag85 awaits structural determination.

Comparison of the Ag85C-$CyC_{8\beta}$ structure with that of Ag85C-ebselen (PDB entry 4QDU (27)) shows that the mode of inhibition triggered by $CyC_{8\beta}$ is different. Ebselen indeed covalently modifies Cys^{209}, which is 13 Å away from the catalytic

Ser^{124} (Fig. 6*C*). Inhibition by ebselen and its derivatives (azido ebselen and adamantyl ebselen) is mediated by inducing structural rearrangements of helix α9 and the loop between helices 9 and 10 that ends in destabilizing the hydrogen bond network of the active site (27, 28, 45). Comparison of the crystal structures of Ag85C-$CyC_{8\beta}$ and the Ag85C native structure (PDB entry 3HRH) possessing the same space group and crystallized in similar conditions shows that the two structures are identical. The superposition of the two structures yields an overall r.m.s. deviation over 251 residues of about 0.19 Å. Furthermore, no local structural rearrangement was observed (data not shown). As expected, the mode of inhibition of $CyC_{8\beta}$ consists of blocking the active site (31) and not of destabilizing the overall structure and stability of the protein as reported for ebselen and its analogs (27, 45). Furthermore, the mode of action of $CyC_{8\beta}$ is more related to that of the diethyl *p*-nitrophenyl phosphate (DEP), a nonspecific α/β hydrolase inhibitor that covalently modifies the Ser^{124} catalytic residue (17). Superposition of the Ag85C-DEP (PDB entry 1DQY) and Ag85C-$CyC_{8\beta}$ structures highlights the similar positioning of the phosphonate groups of the two inhibitors (Fig. 6*D*).

In summary, the data reported here offer a first look at the potent inhibition of the *M. tuberculosis* Ag85C by cyclipostins and cyclophostin analogs, compounds that effectively inhibit growth of extracellularly and intracellularly replicating *M. tuberculosis* and their mechanism of action. Interestingly, a recent study indicated that these compounds were also effective against clinical isolates of the *M. abscessus* complex (46), mostly encountered in cystic fibrosis patients, and known to be intrinsically resistant to most antitubercular drugs. We anticipate that the high-resolution crystal structure of Ag85C-$CyC_{8\beta}$ will now open the way to the development, through structure-based drug design, of improved inhibitors that target the Ag85 complex in various pathogenic mycobacteria.

Experimental procedures

Mycobacterial strains and growth conditions

M. tuberculosis mc^26230 (47) was grown on Middlebrook 7H10 agar plates containing OADC (oleic acid, albumin, dextrose, catalase) enrichment (Difco) and supplemented with 24 μg/ml pantothenic acid. Liquid cultures were obtained by growing mycobacteria in Middlebrook 7H9 (Difco) supplemented with 10% OADC enrichment, 0.2% (v/v) glycerol, 0.05% (v/v), Tween 80 (Sigma), 24 μg/ml pantothenic acid, and 25 μg/ml kanamycin when required.

Plasmids and DNA manipulations

The *fbpC2* gene, encoding Ag85C, was amplified by PCR from *M. tuberculosis* H37Rv genomic DNA using the forward primer 5′-CTA CTT **CAT ATG** TTC TCT AGG CCC GGT CTT CCA G-3′ (NdeI site in boldface type) and the reverse primer 5′-GAG ATT **CTC GAG** AGC AGC AGG CGC AGC AGG GG-3′ (XhoI site in boldface type). The PCR product was cloned into pET23b cut with NdeI and XhoI (New England Biolabs), enabling the incorporation of a polyhistidine tag in the C terminus of the Ag85C protein. The pET23b-*fbpA* and pET23b-*fbpC1* constructs carrying the genes encoding Ag85A and MPT51, respectively, were described previously (11). A codon-optimized version of the *fbpB* gene, encoding Ag85B, was synthesized (GenScript) and introduced within the pET23a plasmid thanks to the NdeI and XhoI restriction sites, enabling also the incorporation of a polyhistidine tag in the C terminus of the Ag85B protein. The $Ag85C^{S124A}$ mutant was obtained by using the PCR-driven overlap extension method (48). Briefly, two separate PCRs were set up with the Phusion® DNA polymerase (Thermo Fisher Scientific). The first one was set up with the forward primer used to amplify the wildtype *fbpC2* gene and the reverse internal primer 5′-AAG ACC CAC CGC CGC GTT-3′. The second one was set up with a forward internal primer, 5′-AAC GCG GCG GTG GGT CTT **G**CG ATG TCG GGC GGT TCC G-3′, overlapping the internal reverse primer and containing the nucleotide substitution (changed nucleotide in boldface type) with the reverse primer used to amplify the wildtype *fbpC2* gene. The purified PCR products were heterodimerized by heating to 95 °C for 1 min, followed by cooling to 60 °C for 10 min in the presence of Phusion® DNA polymerase and dNTPs to generate a double-stranded hybrid. A last step of PCR was performed with the primers used to amplify the wildtype *fbpC2* gene with the hybrid product obtained in the previous step as template. The mutated *fbpC2* gene was finally cloned like the wildtype gene into pET23b and subjected to DNA sequencing to confirm the proper introduction of the mutation. The coding sequence of the gene *Rv3130c*, which encodes Tgs1 from *M. tuberculosis*, was PCR-amplified using the forward primer 5′-GAG GAG **CCA TGG** aga atc tgta ctt cca ggg AAT GAA TCA CCT AAC GAC ACT TGA CGC-3′ (NcoI site in boldface type, tobacco Etch virus protease cleavage site in lowercase type) and the reverse primer 5′-ACG AGG **AAG CTT** TCA CAC AAC CAG CGA TAG CGC T-3′ (HindIII site in boldface type). The PCR amplicon was treated with NcoI and HindIII and ligated to NcoI-HindIII–linearized pET32a. This plasmid containing the polyhistidine and thioredoxin as fusion tags in the N-terminal position was used to produce soluble recombinant Tgs1.

Expression and purification of the individual Ag85 antigens and MPT51

All four plasmids harboring the *fbpA*, *fbpB*, *fbpC2*, and *fbpC1* genes were used to transform the *E. coli* C41 (DE3) expression strain. Transformed bacteria were grown in Luria-Bertani medium containing ampicillin (200 μg/ml) until the A_{600} reached 0.6. Bacterial cultures were then placed on icy water for 30 min before induction with 1 mM isopropyl β-D-1-thiogalactopyranoside and further incubated at 16 °C for 20 h. Bacterial pellets were collected by centrifugation (6,000 × *g*, 4 °C, 1 h) and resuspended in lysis buffer (50 mM Tris, pH 8.0, 200 mM NaCl, 20 mM imidazole, 5 mM β-mercaptoethanol, 1 mM benzamidine). Lysates were sonicated and clarified by centrifugation (27,000 × *g*, 4 °C, 45 min) before purification by nickel-affinity chromatography with nickel-nitrilotriacetic acid–Sepharose beads and elution with lysis buffer containing 250 mM imidazole without benzamidine (GE Healthcare). Proteins were next dialyzed against 50 mM Tris-HCl, pH 8.0, and 5 mM β-mercaptoethanol buffer and loaded on an anion-exchange HiTrap® Q Fast Flow column (GE Healthcare). The protein was eluted with a linear NaCl gradient. The final step of purification was by

size-exclusion chromatography using a Superdex^{TM} 75 10/300 GL column (GE Healthcare). Proteins were eluted in potassium phosphate buffer (50 mM KH_2PO_4/K_2HPO_4, pH 7.6) for DGAT activity assessments. Ag85C was eluted in a sodium phosphate buffer (50 mM NaH_2PO_4/Na_2HPO_4, pH 6.0) for mycolyltransferase activity assessments and in 50 mM Tris-HCl, pH 8.0, 200 mM NaCl for crystallization experiments and stored at 4 °C.

Expression and purification of Tgs1

The *M. tuberculosis* Tgs1 was overproduced in *E. coli* and purified. Briefly, *E. coli* BL21 Rosetta^{TM} 2 was freshly transformed with pET32a-*tgs1*. Exponentially growing bacteria cultured in 2 liters of NYZ Broth (BD Biosciences) were cooled on icy water for 30 min, and 1 mM isopropyl β-D-1-thiogalactopyranoside was added before incubation at 16 °C for 16 h with agitation (200 rpm). Bacteria were then collected by centrifugation, the medium was discarded, and the pellet was resuspended in lysis buffer containing 10% glycerol, which was maintained for all subsequent buffers used. Lysates were produced and subjected to purification via nickel affinity chromatography. His-tagged tobacco etch virus protease was added to the eluted protein solution at a 1:50 (w/w) ratio, and the mixture was dialyzed overnight before again being subjected to nickel-affinity chromatography. The fraction that flowed through the nickel-nitrilotriacetic acid column, containing tagless Tgs1, was concentrated and subjected to size-exclusion chromatography using a Bio-rad ENrich SEC 650 (Bio-rad) and as buffer 100 mM K_2HPO_4/KH_2PO_4, pH 7.5, supplemented with 400 mM NaCl and 10% glycerol. The fractions containing active Tgs1 were pooled and concentrated to 0.1 mg/ml.

RNA extraction, cDNA production, and quantitative real-time PCR

Mycobacterial RNA was purified using the Nucleospin RNA kit (Macherey Nagel) and assessed for purity on a NanoDrop spectrometer and for integrity using a BioAnalyzer (Agilent). Subsequently, RNA was treated by DNase I (Life Technologies) and converted to cDNA using the SuperScript V reverse transcriptase kit (Life Technologies). Quantitative real-time PCR was performed using the LightCycler 480 SYBR Green master mix (Roche Applied Science) and primers specific to the housekeeping control gene *sigA* (forward, 5′-TGT ACT CGT GCG CAG TAA AG-3′; reverse, 5′-GTC GAA TGT CGG CGT TGA TA-3′) and *fbpC2* (forward, 5′-CAG TTT CTA CAC CGA CTG GTA TC-3′; reverse, 5′-TCT CTC TGG TAA GGA AGG TCT C-3′). Triplicate data were analyzed by the $\Delta\Delta Cp$ method with correction for PCR efficiency.

Western blotting

Lysates of *M. tuberculosis* mc^26230 wildtype or overexpressing Ag85C were prepared and subjected to Western blot analysis as described previously (49).

DGAT and mycolyltransferase assays

The DGAT activity assay was performed for 1 h at 37 °C using a protocol reported earlier (33). Briefly, the reaction mixture was composed of 400 μM 1,2-dipalmitoyl-*sn*-glycerol and a 500 μM concentration of the different acyl donor molecules tested (butanoyl-CoA, octanoyl-CoA, lauroyl-CoA, palmitoyl-CoA, and oleoyl-CoA (Sigma-Aldrich)) in 50 mM potassium phosphate buffer, pH 7.6, containing 2% DMSO. The enzyme concentration in the reaction was 3 μM (0.5 μM in the case of Tgs1). At the end of the assay, an equal volume of DTNB (360 μg/ml) was added to the reaction, and the absorbance was measured at 412 nm with a NanoDrop 2000c spectrophotometer (Thermo Fisher Scientific), enabling the calculation of the specific activity of the enzymes (nmol of TNB produced $\times$ min^{-1} $\times$ mg of $protein^{-1}$).

The mycolyltransferase activity assay was performed for 15 min at 35 °C based on a procedure described previously (27). Measurements were taken every 15 s using a Multimode Microplate Reader POLARstar® Omega (BMG Labtech), and the activity of Ag85C was calculated at the maximum rate of the reaction. The reaction mixture was composed of 50 mM sodium phosphate (pH 6.0) containing 2% DMSO, 4 mM trehalose, and 12.5 μM resorufin butyrate (Sigma-Aldrich). The resorufin butyrate was dissolved in DMSO and diluted 100-fold in the reactions. The enzyme concentration in each reaction was 5.5 μM. Data presented were obtained from three independent experiments and analyzed by non-linear regression using GraphPad Prism version 5 software.

Inhibition of the DGAT and mycolyltransferase activity

$CyC_{7\beta}$, $CyC_{8\beta}$, and CyC_{17} were synthesized as described previously (31, 50). To study the inhibitory effect on DGAT activity, a 30 μM concentration of either Ag85A, Ag85B, Ag85C, or MPT51 was co-incubated with increasing concentrations of $CyC_{7\beta}$, $CyC_{8\beta}$, and CyC_{17} for 1 h at room temperature in a reaction mixture containing 50 mM potassium phosphate buffer (pH 7.6), 10% DMSO, and 0.5 times the critical micelle concentration of *n*-dodecyl β-D-maltoside. Inhibition of the mycolyltransferase activity was determined using 55 μM of Ag85C co-incubated with increasing concentrations of $CyC_{7\beta}$, $CyC_{8\beta}$, and CyC_{17} for 30 min at room temperature in 50 mM sodium phosphate buffer (pH 6.0), 10% DMSO, and 0.5 times the critical micelle concentration of *n*-dodecyl β-D-maltoside. Ag85C and $Ag85C^{S124A}$ pretreated or not with the CyC analogs were further incubated with 10 μM ActivX TAMRA-FP probe (Thermo Fisher Scientific) for 1 h at room temperature in the darkness. The reaction was stopped by adding 5× Laemmli reducing buffer followed by boiling, and proteins were separated by 12% SDS-PAGE. Subsequently, TAMRA FP-labeled proteins were detected by fluorescent gel scanning (TAMRA: λ_{ex} 557 nm, λ_{em} 583 nm) using the Cy®3 filter of a ChemiDoc MP Imager (Bio-Rad) before staining of the gels with Coomassie Brilliant Blue dye.

Overexpression of Ag85C variants in M. tuberculosis

The *Rv0129c* gene was amplified by PCR from *M. tuberculosis* H37Rv genomic DNA using the forward primer 5′-CCC AGC TTG TTG ACA GGG TTC GTG-3′ and the reverse primer 5′-ACC AT**G GAT CC**C TAG GCG CCC TGG GGC GCG-3′ (BamHI site in boldface type). After amplification, the PCR product was digested with BamHI (Promega) and cloned into MscI/BamHI- digested pMV261, thus placing the Rv0129c open reading frame under control of the *hsp60* promoter to yield pMV261-Ag85C. The pMV261-$Ag85C^{S124A}$ mutant plasmid was constructed by the QuikChange method using

pMV261-Ag85C as template, Phusion® DNA polymerase (Thermo Fisher Scientific), the forward primer 5′-GCG GCG GTG GGT CTT **GCG** ATG TCG GGC GGT TCC-3′, and the reverse primer 5′-GGA ACC GCC CGA CAT **CGC** AAG ACC CAC CGC CG-3′ (Ser → Ala mutation in boldface type). The DNA sequence was confirmed by DNA sequencing. *M. tuberculosis* mc^{2}6230 was subsequently electrotransformed with pMV261 as a control, pMV261-Ag85C, or pMV261-Ag85C^{S124A}.

Whole-cell radiolabeling experiments and lipid analysis

To investigate the CyC-induced changes in the lipid profile, increasing drug concentrations were added to exponentially growing *M. tuberculosis* mc^{2}6230 cultures grown in Middlebrook 7H9 supplemented with OADC enrichment and Tween 80 and 20 μg/ml pantothenate for 1 h. Subsequently, metabolic labeling of lipids was performed by adding 1 μCi/ml sodium [2-^{14}C]acetate (56 mCi/mmol; American Radio Chemicals) for an additional 6 h at 37 °C. Cells were harvested and delipidated, as described previously (51). The apolar lipid fraction containing TMM and TDM was separated on a 1D TLC plate using the solvent system chloroform/methanol/water (40:8:1, v/v/v) and revealed after exposure to a film. Similarly, the apolar lipid fraction, which also contains TAG, was separated on a 1D TLC plate using the solvent system petroleum ether/diethyl ether (90:10, v/v) and revealed after exposure to film. Delipidated cells were further processed to extract the arabinogalactan-bound mycolic acids (52) and analyzed by TLC/autoradiography using hexane/ethyl acetate (95:5, v/v) run twice in the first dimension followed by exposure to a film to reveal ^{14}C-labeled mycolic acid methyl esters.

Fluorescent microscopy experiments

Wildtype *M. tuberculosis* mc^{2}6230 or strains harboring either the pMV261-Ag85C or its variant pMV261-Ag85C^{S124A} were stained with Nile Red fluorescent probe (Interchim), as described previously (40). Approximately 7.5 × 10^7 cells (OD 1.5) were collected at 9,000 × *g* for 3 min, washed twice with 500 μl of PBS-Tween 0.05%, and resuspended in 300 μl of PBS. Nile Red (15 μl of a solution at 0.5 mg/ml solubilized in ethanol) was added to the bacterial suspension, which was further incubated for 30 min at 37 °C in the darkness. Cells were then centrifuged, washed twice with PBS-Tween 0.05%, and resuspended in 300 μl of PBS. Bacteria were spotted between a 170-μm-thick coverslip and a 1.5% agarose-PBS pad. Image acquisition was performed with an OLYMPUS FV1000 confocal microscope at $\lambda_{ex}\backslash\lambda_{em}$ = 530/590 ± 10 nm, and images were processed and analyzed using ImageJ.

Mass spectrometry

Mass analyses were performed on a MALDI-TOF-TOF Bruker Ultraflex III spectrometer (Bruker Daltonics, Wissembourg, France) controlled by the Flexcontrol version 3.0 package (Build 51). This instrument was used at a maximum accelerating potential of 25 kV and was operated in linear mode using the *m*/*z* range from 20,000 to 100,000 (LP_66 kDa method). Five external standards (Protein Calibration Standard II, Bruker Daltonics) were used to calibrate each spectrum to a mass accuracy within 200 ppm. Peak picking was performed with Flexanalysis version 3.0 software (Bruker) with an adapted analysis method. To eliminate salts from the samples, 10 μl of each preparation was submitted to a desalting step on a C4 Zip-Tip μcolumn (Millipore). 1 μl of desalted sample was mixed with 1 μl of α-cyano-4-hydroxycinnamic acid matrix in a 50% acetonitrile, 0.3% TFA mixture (1:1, v/v). 1 μl was spotted on the target, dried, and analyzed with the LP_66 kDa method. Peak picking was performed with Flexanalysis version 3.0 software (Bruker) with an adapted analysis method. Parameters used were as follows: SNAP peak detection algorithm, S/N threshold fixed to 6, and a quality factor threshold of 30.

Crystallization, data collection, structure determination, and refinement

Crystals were grown in sitting drops at 18 °C by mixing 0.8 μl of protein (in 50 mM Tris-HCl, pH 8.0, and 200 mM NaCl) at a concentration of 8 mg/ml with 0.8 μl of reservoir solution consisting of 0.2 M magnesium chloride hexahydrate, 0.1 M sodium citrate tribasic dihydrate, pH 5.0, and 10% (w/v) polyethylene glycol 20,000. 1-month-old crystals were then soaked for 24 h with a final concentration in the drop of 5 mM $CyC_{8\beta}$. Crystals were fished with a litholoop and flash-cooled in liquid nitrogen without any cryoprotection. Data collection was performed at the ID-23.1 beamline at the ESRF synchrotron (Grenoble, France). Data were processed with *XDS* (53), and the structure was solved by molecular replacement with the structure of Ag85C as search model (PDB code 3HRH (54)) and using *Phaser* from the *PHENIX* software suite (55). Manual adjustments of the model were performed with *Coot* (56), and the structure was refined to 1.8 Å with *PHENIX*. PDB coordinates and structure factors were deposited in the Protein Data Bank under accession number 5OCJ. Data collection and refinement statistics are displayed in Table 1.

Author contributions—A.V., J.-F.C., S.C., M.B., and L.K. conceptualization; A.V., M.R., P.F., and L.C. data curation; A.V., M.R., P.C.N., P.F., L.C., R.R.P., G.R.G., J.-F.C., S.C., and M.B. investigation; A.V., M.R., P.C.N., P.F., L.C., R.R.P., G.R.G., J.-F.C., S.C., and M.B. methodology; A.V., M.R., P.F., L.C., C.D.S., J.-F.C., S.C., M.B., and L.K. writing-review and editing; P.C.N. visualization; C.D.S. and S.C. resources; M.B. and L.K. supervision; L.K. funding acquisition; L.K. validation; L.K. writing-original draft; L.K. project administration.

Acknowledgments—We thank K. Huygen for kindly providing the 17/4 and 32/15 monoclonal antibodies, W. R. Jacobs, Jr., for M. tuberculosis mc^{2}6230, and P. Santucci for help in fluorescent microscopy experiments. This work benefited from the facilities and expertise of the Platform for Microscopy of IMM. We thank the ESRF and SLS beamline staffs for support during data collection. Mass spectrometry analyses were done using the mass spectrometry facility of Marseille Proteomics, supported by IBISA (Infrastructures Biologie Santé et Agronomie), the Cancéropôle PACA, the Provence-Alpes-Côte d'Azur Region, the Institut Paoli-Calmettes, and the Centre de Recherche en Cancérologie de Marseille.

References

1. Dheda, K., Gumbo, T., Maartens, G., Dooley, K. E., McNerney, R., Murray, M., Furin, J., Nardell, E. A., London, L., Lessem, E., Theron, G., van Helden, P., Niemann, S., Merker, M., Dowdy, D., *et al.* (2017) The epidemiology,

pathogenesis, transmission, diagnosis, and management of multidrug-resistant, extensively drug-resistant, and incurable tuberculosis. *Lancet Respir. Med.* **5,** 291–360 CrossRef Medline
2. Barry, C. E., 3rd, and Mdluli, K. (1996) Drug sensitivity and environmental adaptation of mycobacterial cell wall components. *Trends Microbiol.* **4,** 275–281 CrossRef Medline
3. Brennan, P. J., and Nikaido, H. (1995) The envelope of mycobacteria. *Annu. Rev. Biochem.* **64,** 29–63 CrossRef Medline
4. Mikusová, K., Slayden, R. A., Besra, G. S., and Brennan, P. J. (1995) Biogenesis of the mycobacterial cell wall and the site of action of ethambutol. *Antimicrob. Agents Chemother.* **39,** 2484–2489 CrossRef Medline
5. Vilchèze, C., Wang, F., Arai, M., Hazbón, M. H., Colangeli, R., Kremer, L., Weisbrod, T. R., Alland, D., Sacchettini, J. C., and Jacobs, W. R. (2006) Transfer of a point mutation in *Mycobacterium tuberculosis inhA* resolves the target of isoniazid. *Nat. Med.* **12,** 1027–1029 CrossRef Medline
6. Matsumoto, M., Hashizume, H., Tomishige, T., Kawasaki, M., Tsubouchi, H., Sasaki, H., Shimokawa, Y., and Komatsu, M. (2006) OPC-67683, a nitro-dihydro-imidazooxazole derivative with promising action against tuberculosis *in vitro* and in mice. *PLoS Med.* **3,** e466 CrossRef Medline
7. Tahlan, K., Wilson, R., Kastrinsky, D. B., Arora, K., Nair, V., Fischer, E., Barnes, S. W., Walker, J. R., Alland, D., Barry, C. E., 3rd, and Boshoff, H. I. (2012) SQ109 targets MmpL3, a membrane transporter of trehalose monomycolate involved in mycolic acid donation to the cell wall core of *Mycobacterium tuberculosis*. *Antimicrob. Agents Chemother.* **56,** 1797–1809 CrossRef Medline
8. Harth, G., Lee, B. Y., Wang, J., Clemens, D. L., and Horwitz, M. A. (1996) Novel insights into the genetics, biochemistry, and immunocytochemistry of the 30-kilodalton major extracellular protein of *Mycobacterium tuberculosis*. *Infect. Immun.* **64,** 3038–3047 Medline
9. Belisle, J. T., Vissa, V. D., Sievert, T., Takayama, K., Brennan, P. J., and Besra, G. S. (1997) Role of the major antigen of *Mycobacterium tuberculosis* in cell wall biogenesis. *Science* **276,** 1420–1422 CrossRef Medline
10. Jackson, M., Raynaud, C., Lanéelle, M. A., Guilhot, C., Laurent-Winter, C., Ensergueix, D., Gicquel, B., and Daffé, M. (1999) Inactivation of the antigen 85C gene profoundly affects the mycolate content and alters the permeability of the *Mycobacterium tuberculosis* cell envelope. *Mol. Microbiol.* **31,** 1573–1587 CrossRef Medline
11. Kremer, L., Maughan, W. N., Wilson, R. A., Dover, L. G., and Besra, G. S. (2002) The *M. tuberculosis* antigen 85 complex and mycolyltransferase activity. *Lett. Appl. Microbiol.* **34,** 233–237 CrossRef Medline
12. Armitige, L. Y., Jagannath, C., Wanger, A. R., and Norris, S. J. (2000) Disruption of the genes encoding antigen 85A and antigen 85B of *Mycobacterium tuberculosis* H37Rv: effect on growth in culture and in macrophages. *Infect. Immun.* **68,** 767–778 Medline
13. Nguyen, L., Chinnapapagari, S., and Thompson, C. J. (2005) FbpA-dependent biosynthesis of trehalose dimycolate is required for the intrinsic multidrug resistance, cell wall structure, and colonial morphology of *Mycobacterium smegmatis*. *J. Bacteriol.* **187,** 6603–6611 CrossRef Medline
14. Puech, V., Guilhot, C., Perez, E., Tropis, M., Armitige, L. Y., Gicquel, B., and Daffé, M. (2002) Evidence for a partial redundancy of the fibronectin-binding proteins for the transfer of mycoloyl residues onto the cell wall arabinogalactan termini of *Mycobacterium tuberculosis*: redundancy of fibronectin-binding proteins in *M. tuberculosis*. *Mol. Microbiol.* **44,** 1109–1122 CrossRef Medline
15. Wilson, R. A., Rai, S., Maughan, W. N., Kremer, L., Kariuki, B. M., Harris, K. D. M., Wagner, T., Besra, G. S., and Fütterer, K. (2003) Crystallization and preliminary X-ray diffraction data of *Mycobacterium tuberculosis* FbpC1 (Rv3803c). *Acta Crystallogr. D Biol. Crystallogr.* **59,** 2303–2305 CrossRef Medline
16. Wilson, R. A., Maughan, W. N., Kremer, L., Besra, G. S., and Fütterer, K. (2004) The structure of *Mycobacterium tuberculosis* MPT51 (FbpC1) defines a new family of non-catalytic α/β hydrolases. *J. Mol. Biol.* **335,** 519–530 CrossRef Medline
17. Ronning, D. R., Klabunde, T., Besra, G. S., Vissa, V. D., Belisle, J. T., and Sacchettini, J. C. (2000) Crystal structure of the secreted form of antigen 85C reveals potential targets for mycobacterial drugs and vaccines. *Nat. Struct. Biol.* **7,** 141–146 CrossRef Medline
18. Anderson, D. H., Harth, G., Horwitz, M. A., and Eisenberg, D. (2001) An interfacial mechanism and a class of inhibitors inferred from two crystal structures of the *Mycobacterium tuberculosis* 30 kDa major secretory protein (Antigen 85B), a mycolyl transferase. *J. Mol. Biol.* **307,** 671–681 CrossRef Medline
19. Ronning, D. R., Vissa, V., Besra, G. S., Belisle, J. T., and Sacchettini, J. C. (2004) *Mycobacterium tuberculosis* antigen 85A and 85C structures confirm binding orientation and conserved substrate specificity. *J. Biol. Chem.* **279,** 36771–36777 CrossRef Medline
20. Daffé, M. (2000) The mycobacterial antigens 85 complex: from structure to function and beyond. *Trends Microbiol.* **8,** 438–440 CrossRef Medline
21. Favrot, L., and Ronning, D. R. (2012) Targeting the mycobacterial envelope for tuberculosis drug development. *Expert Rev. Anti Infect. Ther.* **10,** 1023–1036 CrossRef Medline
22. Jackson, M., McNeil, M. R., and Brennan, P. J. (2013) Progress in targeting cell envelope biogenesis in *Mycobacterium tuberculosis*. *Future Microbiol.* **8,** 855–875 CrossRef Medline
23. Rose, J. D., Maddry, J. A., Comber, R. N., Suling, W. J., Wilson, L. N., and Reynolds, R. C. (2002) Synthesis and biological evaluation of trehalose analogs as potential inhibitors of mycobacterial cell wall biosynthesis. *Carbohydr. Res.* **337,** 105–120 CrossRef Medline
24. Barry, C. S., Backus, K. M., Barry, C. E., 3rd, and Davis, B. G. (2011) ESI-MS assay of *M. tuberculosis* cell wall antigen 85 enzymes permits substrate profiling and design of a mechanism-based inhibitor. *J. Am. Chem. Soc.* **133,** 13232–13235 CrossRef Medline
25. Warrier, T., Tropis, M., Werngren, J., Diehl, A., Gengenbacher, M., Schlegel, B., Schade, M., Oschkinat, H., Daffe, M., Hoffner, S., Eddine, A. N., and Kaufmann, S. H. E. (2012) Antigen 85C inhibition restricts *Mycobacterium tuberculosis* growth through disruption of cord factor biosynthesis. *Antimicrob. Agents Chemother.* **56,** 1735–1743 CrossRef Medline
26. Scheich, C., Puetter, V., and Schade, M. (2010) Novel small molecule inhibitors of MDR *Mycobacterium tuberculosis* by NMR fragment screening of antigen 85C. *J. Med. Chem.* **53,** 8362–8367 CrossRef Medline
27. Favrot, L., Grzegorzewicz, A. E., Lajiness, D. H., Marvin, R. K., Boucau, J., Isailovic, D., Jackson, M., and Ronning, D. R. (2013) Mechanism of inhibition of *Mycobacterium tuberculosis* antigen 85 by ebselen. *Nat. Commun.* **4,** 2748 Medline
28. Favrot, L., Lajiness, D. H., and Ronning, D. R. (2014) Inactivation of the *Mycobacterium tuberculosis* antigen 85 complex by covalent, allosteric inhibitors. *J. Biol. Chem.* **289,** 25031–25040 CrossRef Medline
29. Nguyen, P. C., Delorme, V., Bénarouche, A., Martin, B. P., Paudel, R., Gnawali, G. R., Madani, A., Puppo, R., Landry, V., Kremer, L., Brodin, P., Spilling, C. D., Cavalier, J.-F., and Canaan, S. (2017) Cyclipostins and cyclophostin analogs as promising compounds in the fight against tuberculosis. *Sci. Rep.* **7,** 11751 CrossRef Medline
30. Dupont, C., Viljoen, A., Dubar, F., Blaise, M., Bernut, A., Pawlik, A., Bouchier, C., Brosch, R., Guérardel, Y., Lelièvre, J., Ballell, L., Herrmann, J.-L., Biot, C., and Kremer, L. (2016) A new piperidinol derivative targeting mycolic acid transport in *Mycobacterium abscessus*. *Mol. Microbiol.* **101,** 515–529 CrossRef Medline
31. Point, V., Malla, R. K., Diomande, S., Martin, B. P., Delorme, V., Carriere, F., Canaan, S., Rath, N. P., Spilling, C. D., and Cavalier, J.-F. (2012) Synthesis and kinetic evaluation of cyclophostin and cyclipostins phosphonate analogs as selective and potent inhibitors of microbial lipases. *J. Med. Chem.* **55,** 10204–10219 CrossRef Medline
32. Liu, Y., Patricelli, M. P., and Cravatt, B. F. (1999) Activity-based protein profiling: the serine hydrolases. *Proc. Natl. Acad. Sci. U.S.A.* **96,** 14694–14699 CrossRef Medline
33. Elamin, A. A., Stehr, M., Spallek, R., Rohde, M., and Singh, M. (2011) The *Mycobacterium tuberculosis* Ag85A is a novel diacylglycerol acyltransferase involved in lipid body formation. *Mol. Microbiol.* **81,** 1577–1592 CrossRef Medline
34. Lakey, D. L., Voladri, R. K., Edwards, K. M., Hager, C., Samten, B., Wallis, R. S., Barnes, P. F., and Kernodle, D. S. (2000) Enhanced production of recombinant *Mycobacterium tuberculosis* antigens in *Escherichia coli* by replacement of low-usage codons. *Infect. Immun.* **68,** 233–238 CrossRef Medline

35. Viljoen, A., Blaise, M., de Chastellier, C., and Kremer, L. (2016) MAB_3551c encodes the primary triacylglycerol synthase involved in lipid accumulation in *Mycobacterium abscessus*. *Mol. Microbiol.* **102,** 611–627 CrossRef Medline
36. Daniel, J., Deb, C., Dubey, V. S., Sirakova, T. D., Abomoelak, B., Morbidoni, H. R., and Kolattukudy, P. E. (2004) Induction of a novel class of diacylglycerol acyltransferases and triacylglycerol accumulation in *Mycobacterium tuberculosis* as it goes into a dormancy-like state in culture. *J. Bacteriol.* **186,** 5017–5030 CrossRef Medline
37. Huygen, K., Lozes, E., Gilles, B., Drowart, A., Palfliet, K., Jurion, F., Roland, I., Art, M., Dufaux, M., and Nyabenda, J. (1994) Mapping of TH1 helper T-cell epitopes on major secreted mycobacterial antigen 85A in mice infected with live *Mycobacterium bovis* BCG. *Infect. Immun.* **62,** 363–370 Medline
38. Daniel, J., Maamar, H., Deb, C., Sirakova, T. D., and Kolattukudy, P. E. (2011) *Mycobacterium tuberculosis* uses host triacylglycerol to accumulate lipid droplets and acquires a dormancy-like phenotype in lipid-loaded macrophages. *PLoS Pathog.* **7,** e1002093 CrossRef Medline
39. Garton, N. J., Christensen, H., Minnikin, D. E., Adegbola, R. A., and Barer, M. R. (2002) Intracellular lipophilic inclusions of mycobacteria *in vitro* and in sputum. *Microbiol. Read. Engl.* **148,** 2951–2958 CrossRef Medline
40. Dhouib, R., Ducret, A., Hubert, P., Carrière, F., Dukan, S., and Canaan, S. (2011) Watching intracellular lipolysis in mycobacteria using time lapse fluorescence microscopy. *Biochim. Biophys. Acta* **1811,** 234–241 CrossRef Medline
41. Kalscheuer, R., and Steinbüchel, A. (2003) A novel bifunctional wax ester synthase/acyl-CoA:diacylglycerol acyltransferase mediates wax ester and triacylglycerol biosynthesis in *Acinetobacter calcoaceticus* ADP1. *J. Biol. Chem.* **278,** 8075–8082 CrossRef Medline
42. Peyron, P., Vaubourgeix, J., Poquet, Y., Levillain, F., Botanch, C., Bardou, F., Daffé, M., Emile, J.-F., Marchou, B., Cardona, P.-J., de Chastellier, C., and Altare, F. (2008) Foamy macrophages from tuberculous patients' granulomas constitute a nutrient-rich reservoir for *M. tuberculosis* persistence. *PLoS Pathog.* **4,** e1000204 CrossRef Medline
43. Santucci, P., Bouzid, F., Smichi, N., Poncin, I., Kremer, L., De Chastellier, C., Drancourt, M., and Canaan, S. (2016) Experimental models of foamy macrophages and approaches for dissecting the mechanisms of lipid accumulation and consumption during dormancy and reactivation of tuberculosis. *Front. Cell. Infect. Microbiol.* **6,** 122 Medline
44. Lehmann, J., Cheng, T.-Y., Aggarwal, A., Park, A. S., Zeiler, E., Raju, R. M., Akopian, T., Kandror, O., Bach, N. C., Sacchettini, J. C., Moody, D. B., Rubin, E. J., and Sieber, S. A. (2018) An antibacterial β-lactone kills *Mycobacterium tuberculosis* by infiltrating mycolic acid biosynthesis. *Angew. Chem. Int. Ed. Engl.* **57,** 348–353 Medline
45. Goins, C. M., Dajnowicz, S., Thanna, S., Sucheck, S. J., Parks, J. M., and Ronning, D. R. (2017) Exploring covalent allosteric inhibition of antigen 85C from *Mycobacterium tuberculosis* by ebselen derivatives. *ACS Infect. Dis.* **3,** 378–387 CrossRef Medline
46. Nguyen, P. C., Madani, A., Santucci, P., Martin, B. P., Paudel, R., Delattre, S., Herrmann, J.-L., Spilling, C. D., Kremer, L., Canaan, S., and Cavalier, J.-F. (2017) Cyclophostin and cyclipostins analogs, new promising molecules to treat mycobacterial-related diseases. *Int. J. Antimicrob. Agents* 10.1016/j.ijantimicag.2017.12.001 CrossRef Medline
47. Sambandamurthy, V. K., Derrick, S. C., Hsu, T., Chen, B., Larsen, M. H., Jalapathy, K. V., Chen, M., Kim, J., Porcelli, S. A., Chan, J., Morris, S. L., and Jacobs, W. R. (2006) *Mycobacterium tuberculosis* ΔRD1 ΔpanCD: a safe and limited replicating mutant strain that protects immunocompetent and immunocompromised mice against experimental tuberculosis. *Vaccine* **24,** 6309–6320 CrossRef Medline
48. Heckman, K. L., and Pease, L. R. (2007) Gene splicing and mutagenesis by PCR-driven overlap extension. *Nat. Protoc.* **2,** 924–932 CrossRef Medline
49. Kremer, L., Dover, L. G., Morbidoni, H. R., Vilchèze, C., Maughan, W. N., Baulard, A., Tu, S.-C., Honoré, N., Deretic, V., Sacchettini, J. C., Locht, C., Jacobs, W. R., Jr., and Besra, G. S. (2003) Inhibition of InhA activity, but not KasA activity, induces formation of a KasA-containing complex in mycobacteria. *J. Biol. Chem.* **278,** 20547–20554 CrossRef Medline
50. Vasilieva, E., Dutta, S., Malla, R. K., Martin, B. P., Spilling, C. D., and Dupureur, C. M. (2015) Rat hormone sensitive lipase inhibition by cyclipostins and their analogs. *Bioorg. Med. Chem.* **23,** 944–952 CrossRef Medline
51. Kremer, L., Guérardel, Y., Gurcha, S. S., Locht, C., and Besra, G. S. (2002) Temperature-induced changes in the cell-wall components of *Mycobacterium thermoresistibile*. *Microbiol. Read. Engl.* **148,** 3145–3154 CrossRef Medline
52. Coxon, G. D., Craig, D., Corrales, R. M., Vialla, E., Gannoun-Zaki, L., and Kremer, L. (2013) Synthesis, antitubercular activity and mechanism of resistance of highly effective thiacetazone analogues. *PLoS One* **8,** e53162 CrossRef Medline
53. Kabsch, W. (2010) Integration, scaling, space-group assignment and post-refinement. *Acta Crystallogr. D Biol. Crystallogr.* **66,** 133–144 CrossRef Medline
54. Sanki, A. K., Boucau, J., Umesiri, F. E., Ronning, D. R., and Sucheck, S. J. (2009) Design, synthesis and biological evaluation of sugar-derived esters, α-ketoesters and α-ketoamides as inhibitors for *Mycobacterium tuberculosis* antigen 85C. *Mol. Biosyst.* **5,** 945–956 CrossRef Medline
55. Adams, P. D., Afonine, P. V., Bunkóczi, G., Chen, V. B., Echols, N., Headd, J. J., Hung, L.-W., Jain, S., Kapral, G. J., Grosse Kunstleve, R. W., McCoy, A. J., Moriarty, N. W., Oeffner, R. D., Read, R. J., Richardson, D. C., *et al.* (2011) The Phenix software for automated determination of macromolecular structures. *Methods* **55,** 94–106 CrossRef Medline
56. Emsley, P., Lohkamp, B., Scott, W. G., and Cowtan, K. (2010) Features and development of Coot. *Acta Crystallogr. D Biol. Crystallogr.* **66,** 486–501 CrossRef Medline

Cyclipostins and cyclophostin analogs inhibit the antigen 85C from *Mycobacterium tuberculosis* both *in vitro* and *in vivo*

Albertus Viljoen, Matthias Richard, Phuong Chi Nguyen, Patrick Fourquet, Luc Camoin, Rishi R. Paudal, Giri R. Gnawali, Christopher D. Spilling, Jean-François Cavalier, Stéphane Canaan, Mickael Blaise and Laurent Kremer

J. Biol. Chem. 2018, 293:2755-2769.
doi: 10.1074/jbc.RA117.000760 originally published online January 4, 2018